BNL-26094
CONF-790574--1

Scanning Reference Electrode Techniques in Localized Corrosion*

H.S. Isaacs and B. Vyas

Brookhaven National Laboratory

Upton, New York 11973

April 1979

*Research carried out under the auspices of the United States Department of Energy under Contract No. EY-76-C-02-0016

DISCLAIMER

TABLE OF CONTENTS

LIST OF FIGURES

Scanning Reference Electrode Teciques in Localized Corrosion*

H.S. Isaacs and B. Vyas

Brookhaven National Laboratory

Upton, New York 11973

ABSTRACT

The principles, advantages, and implementations of scanning reference electrode techniques are reviewed. Data related to pitting, intergranular corrosion, welds and stress corrosion cracking are presented. The technique locates the position of localized corrosion and can be used to monitor the development of corrosion and changes in the corrosion rate under a wide range of conditions.

*Research carried out under the auspices of the United States Department of Energy.

INTRODUCTION

The definition of localized corrosion usually is restricted to specific types of attack often related to the presence of chlorides. This definition may be broadened to incorporate all other cases where corrosion at specific areas of the metal surface takes place. General corrosion rates in most systems have been measured and design allowance can be made for the metal losses during the expected life of the system. Problems arise when the corrosion becomes localized and the penetration rate of the metal is orders of magnitude greater than the predicted general corrosion and, in numerable cases is only identified after failure. Localized forms of corrosion, therefore, take a far greater toll than the incorrect choice of materials that give unacceptable general corrosion.

During localized corrosion,[1,2] the electrochemical dissolution is well separated from the cathodic reactions. This makes an *in situ* study of the anodic and cathodic reactions amenable to direct measurement in contrast to general corrosion where the reactions can take place in close proximity. The aim of this investigation is to clearly separate the anodic and cathodic reactions without interfering with the processes taking place, or, alter them to any extent whereby they no longer relate to conditions during exposure. *In situ* measurements such as mapping of potentials in solution or the physical separation of anodic and cathodic areas and measuring the currents flowing between them have been used successfully to identify the processes during corrosion.

Other methods such as weight loss or penetration rates have also been used but these require periodic removal of the metal from the corroding environment. The periodic removal can alter the progress of corrosion or initiate changes in the processes involved. Thus, the measurements do not necessarily represent a single progression of the reaction but possibly the integrated effect of a repet-

itive process. For example, during pitting the pits may repassivate on removal from the corrosive environment and reinitiate on subsequent exposure. In the case of stress corrosion cracking, the uncorroded area may act as the cathode, and, when cathodic polarization is limiting, interaction between the growth rates of the various cracks would be expected. However, when the anodic process is slow or when the cathode is at the crack wall, no interaction between the cracks would occur. The identification of these effects would require a large number of samples because of the required statistics, and even then it would be extremely difficult to extract the rate processes or the electrochemistry taking place.

In a large number of studies, sections of samples have been used to separate the anodic and cathodic processes.[3-6] In an early work related to the water line corrosion,[3] the corroding section of the sample was separated from the partially immersed cathodic portion. The currents between the shorted pieces gave rates which correlated well with the observed weight losses. The behavior of welds has also been studied using similar techniques.[4] The welds were sectioned or masked to give representative parts parallel with the weld direction. Separate sections of plates have also been used to investigate pitting corrosion.[5] Measurements were conducted on the relation and variations of current between the different sections during pitting corrosion and demonstrate the existence of a marked dependence between pit size and its stability.

Areas around a weld have been studied separately using a liquid drop drawn across the sample. The potential variations and the polarization characteristics as a function of the drop position were measured.[7] In another study,[8] an insulating coating over a weld area was perforated with a micro-

hardness indentor, and a liquid drop was placed over the perforation. The potential and the polarization characteristics of the underlying deformed and wetted metal was measured.

The flow of current from the anodic to the cathodic areas can also be determined without sectioning samples. In an early work on water line corrosion, Evans and Agar[9] calculated the current from the measured equipotential lines associated with the flow of current during the corrosion of zinc. A scanning reference electrode technique (SRET) was used to measure the potential variation in the solution. An agreement of within 10% was obtained between the measured corrosion rates from weight loss and the calculations from the equipotential surfaces.

Jaenicke and Bonhoeffer,[10,11] Copson[12] and Rozenfeld[13] have measured the potential distribution around galvanic couples and calculated the corrosion rates and the surface current density distributions. Measurements of potential distribution during corrosion of bismuth-cadmium and zinc-aluminum alloys were also studied.[11] More recent measurements of couples of iron and copper have been conducted by Heldebrand and Schwenk.[14]

THEORY

Aqueous corrosion of metals is an electrochemical process involving anodic oxidation of the metal and cathodic reduction of species from the solution. During localized corrosion, the two processes usually take place at well separated areas. The flow of electrons within the metallic phase does not involve significant ohmic potential differences because of the high conductivity of the metal. The flow of current within the aqueous phase, carried by ions, is associated with small potential changes between the anodic and cathodic areas.

Figure 1 shows a schematic of the flow of current in the electrolyte from a localized anodic to the surrounding cathodic areas and equipotentials set up around the localized electrode. By scanning a "passive" reference probe with a fine capillary tip parallel to and in close proximity to the metal surface the potential distribution in the liquid can be measured. The potential changes are most rapid over the localized electrode and a potential maximum or minimum is observed over its center. In the SRET work presented here, the sign convention adopted is opposite to that generally used in order to show anodic areas as potential peaks and cathodic areas as minima. Thus, the SRET is an in situ technique to locate the anodic and cathodic sites and study the electrochemical processes during localized corrosion, without altering the processes taking place, changing the local environment over the corrosion site or influencing the rate of corrosion.

The distribution of potential and current can be determined theoretically from the Laplace equation.

$$\nabla^2 E = 0 \qquad \text{(i)}$$

and Ohm's Law

$$i = -K\nabla E \qquad \text{(ii)}$$

where E, i, and K are the potential, the current density and the solution conductivity. The boundary conditions for the solution of these equations depends on the polarization characteristics of the anodic and cathodic areas. If either area has a high polarization characteristic, low currents will flow in solution,

and, hence, there will be little potential variations between anode and cathode. With high currents, a greater variation of potential will occur. The product of the polarization resistances $(\frac{\Delta V}{\Delta i})$ and the electrolyte conductivity has the dimension of length

$$L = K \frac{\Delta V}{\Delta i} \qquad \text{(iii)}$$

and has been used to determine the potential variations in corroding systems.[15-19]

It should be emphasized that the SRET does not directly measure the potential variations of the metal surface but responds to current variations in solution. These currents are more dependent on the polarization characteristics of the metal surface rather than the surface potential. This can be demonstrated by the following hypothetical examples.

In Fig. 2(a), three Evans type polarization curves are shown. In A, anodic and cathodic partial polarization curves are given by the dashed lines representing the reactions on a passive metal surface (e.g., iron in a chloride solution below its pitting potential). The full lines represent the net polarization curves. In B, anodic polarization curves representing anodic behavior of a localized anodic cell (e.g., a large pit) for two different conditions, one (I) having a greater polarization characteristic than the other (II). The third Evans type diagram, C, could be for a noble metal (e.g., a Pt coating on iron). The cathodic curves in Fig. 3(a) A and C could arise from oxygen reduction and, if equal in area, would show the same currents when limiting concentration polarization is reached. These three areas are considered to be present on a single

metal surface separated by an insulating coating as in Fig. 3(b), (c) and (e), where the 'iron' forms the base of a shallow container holding a highly conducting chloride containing electrolyte. In Fig. 3(b) the solutions in contact with areas A, B, and C are separarated from each other and have the respective Evans type diagrams shown in Fig. 3(a). Each area is at its open circuit potential and measurements of the potential as a function of the position in the solution can be represented by Fig. 3(c). If these separations are removed, two conditions can arise depending on the anodic behavior of area B. If the lower polarization is considered then the polarization of the three areas would be close to potential E_1 in Fig. 3(a). The currents from the anodic area B would flow to both A and C and the potentials developed in the solution are shown by equipotential lines in Fig. 3(d). If the potential was measured at a fixed distance from the metal surface above the coating using the SRET, then the potential variations would be similar to the curve shown in Fig. 3(e). The magnitude of these potential variations cover a range ΔE, which is much smaller than the potential range shown in Fig. 3(c).

Under conditions where the anodic area, B, has the larger polarization (I) the potential of the three areas would be close to E_2 shown in Fig. 3(a). This potential is equal to E_A, the open circuit potential of area A, and under this condition no currents will flow to or from A. The equipotential lines for this condition is shown in Fig. 3(f). The shape of the potential variations from the SRET is shown in Fig. 3(g). It should be noted that no potential variations are observed when scanning above area A and the potential measurements would not be capable of distinguishing whether the probe is directly over the area A or the coatings adjacent to it. A similar condition could be achieved if area A is placed between B and C and if the coating was thin it would once again not

distinguish between the presence of a coating or the passive metal surface under the scanning reference electrode from the potential variations. This analysis clearly demonstrates that the SRET only responds to potential variations in the solution, which are associated with the flow of current, and does not relate directly to the potentials of the metal surfaces or the coating.

EXPERIMENTAL TECHNIQUE

The potential fields generated in the electrolyte due to local corrosion sites can be measured by scanning a microtip reference electrode over a horizontal exposed surface facing up. The equipment built at Brookhaven National Laboratory is shown schematically in Fig. 3.[20,21] The microtip reference electrode is held by a mechanical stage attached to low friction, linear bearings for smooth motion in the X and Y direction, and driven by two stepping motors. The mechanical stage can be automatically programmed to scan both in the X and Y directions parallel to the specimen surface. The lenth of the X direction can be varied up to 26 mm, and, at each end of the X scan, the Y direction can be shifted to a set value (from 30 μm to 200 μm). Thus, an area of the surface is scanned by a rectangular wave. The linear speed of the scan in the X direction can be varied from 0.1 mm/sec to 300 mm/sec.

Alternatively, potential fields on cylindrical samples can be obtained by keeping the probe stationary while rotating the sample.[22,23] The microtip reference electrode measures the potential variations along the circumference of the sample as the potential field around the sample rotates with the sample. A schematic of such an instrument is shown in Fig. 4.[23] A motor is used to rotate a cylindrical metal specimen in the electrolyte such that the rotational motion of the sample is synchronized to produce a signal which is proportional to the angular position of the sample with respect to the probe. The microtip

reference electrode is made to scan in the vertical direction (parallel to the cylindrical axis). If the signal of the sample rotation is fed to the X direction and signal of scan of the probe to the Y direction, the surface scan of the cylindrical specimen is obtained. The size of the area examined on the specimen surface can be controlled by regulating the length over which the microtip reference electrode moves along the axis of the sample and controlling the time per revolution of the specimen.

The most important parameter in the measurement of the potential fields is the distance between the microtip reference electrode and the specimen surface which must be held constant during a given experiment. This is achieved by attaching the sample to a stage with three independent rotations when flat samples are studied. Also, mechanical vibrations are kept to a minimum by attaching the mechanical stage to a cast iron stand which is placed on a vibration free table. In the case of a rotating sample, it is necessary that the motor, rotating shaft, and the sample lie on the same axis so that there is no eccentricity of the rotation. Also, the whole apparatus should be made as rigid as possible.[22]

The potential field in the electrolyte during localized corrosion is the difference in the potential measured by the microtip reference electrode and a reference electrode placed more than 10 mm away from the sample surface. The two signals are fed into a differential electrometer and the resultant potential amplified to the desired amount. The potential fields can be plotted on a X-Y recorder by feeding the signal from the X position of the motor to the X amplifier of the recorder the sum of the Y position of the motor and the amplified potential difference to the Y amplifier of the recorder. Thus, one obtains a two dimensional plot of the potential field variations at a plane parallel to the

sample surface. The signals can also be recorded on a storage oscilloscope and photographed. Alternately, the amplified potential difference can modulate the intensity of the cathode ray tube of an oscilloscope,[20] or plot the equipotential lines from an analyzer.[23]

A third scanning technique[24] incorporates two adjacent reference electrode probes to determine the currents flowing from the pits. Two scans are required for each measurement. One scan, having two probes close together displaced horizontally, gives the potential fields parallel to the specimen surface. In the other scan, the probes are displaced vertically to determine the field perpendicular to the surface. The vector sum of the fields indicates the magnitude and direction of the current flow, and summation over the active area is used to estimate the total currents from the anodic to the cathodic areas. This technique only integrates the current flowing across the plane of the potential measurement and does not include the currents flowing below the probes. These latter currents can be a significant fraction of the total current. Fig. 5 shows the two fields normal and parallel to the surface over a pit on stainless steel.

Calibration

In order to obtain a quantitative value of the local corrosion currents, it is necessary to obtain a relation between the potential peak and the local current. This may be obtained theoretically by equations (ii) and (iii)[15] or determined experimentally. In view of the lack of data relating the polarization characteristics of the systems studied, this relation was determined using a model electrochemical cell consisting of a localized anode in a large cathode.

A platinum sheet, 25 μm thick, was sandwiched between two copper blocks 10 mm wide and 10 mm long. The platinum was electrically insulated from the copper

by two mylar sheets 125 μm thick. The platinum was made the anode, and the copper the cathode. Platinum does not dissolve in the electrolyte and, hence, maintains its structural shape. The probe was scanned parallel to the surface of this model cell, across the anode and the cathode, at various sample to probe distances, d, in electrolytes of different conductance.

The peaks obtained for an applied anodic current of 1 μA through the platinum in 0.001N H_2SO_4 as a function of d are shown in Fig. 6. If the probe is too far from the specimen surface, then either the signal is lost or the peaks are small and broad. As d decreases, the peak height increases and the width of the peak decreases giving a clear location of the local corrosion site. As anticipated, these results are consistent with the potential field generated from a local region shown in Fig. 1. Therefore, for a clear determination of the corrosion site the probe should be held close to the sample surface. However, the distance between the probe and metal surface should not be less than the outer tip diameter of the probe, or else it will disturb the potential distribution in the electrolyte.[25] For kinetic studies, a constant value of d must be maintained to obtain meaningful relation between the peak height and the local current.

The effect of electrolyte conductivity on the peak height is shown in Fig. 7. The peak heights, with d=25μ and for anodic currents varied over two orders of magnitude increased with decrease in electrolyte conductivity. Also for a given electrolyte conductivity, there is a linear relationship between the peak height and the magnitude of the applied current. Thus, the peak heights give a direct measure of the intensity of the corrosion currents originating from the anodic sites.

Finally, the effect of the local area on the magnitude and shape of the peak is shown in Fig. 8. The peak height over the local region increases with increase in area due to the increase in the local current up to an area where the anode becomes large (0.5 mm) and cannot be treated as a local region. Also, it is observed that the maximum in the peak lies over the center of the local area. Thus the peak shape gives an indication of the area of the local region.

Sensitivity and Resolution

The sensitivity of the SRET, i.e. the ability to unambiguously determine very small corrosion currents originating from localized regions and the resolution, i.e. the ability to distinguish between two anodic sites close to each other, are mainly governed by the distance between the probe and specimen surface and the conductivity of the solution, as discussed above. However, in a given experiment, the choice of the electrolyte may be limited by the type of localized corrosion to be studied. Also, the distance d is limited to the diameter of the probe tip. A decrease in the probe tip diameter increases the sensitivity and resolution of the technique. However, a very fine tip has a very high impedance which increases the electrical noise and decreases the response time. Therefore, proper compromise should be made for the choice of the probe tip diameter.

The resolution of the SRET is not only dependent on the proximity of two corroding sites but the magnitude of the corrosion current from each site. A schematic of the potential peaks obtained from two adjacent points, for various corrosion conditions is shown in Fig. 10. If the corrosion currents from the two anodic sites are low, the potential peaks are small and broad. Hence, these can be resolved only if d is small. If the potential field from the two corroding sites are large, one does not obtain separate distinguished peaks, but

two small peaks on a large broad peak. However, if one of the sites corrodes much faster than the other site, one observes only a change in the slope of the larger potential peak at the point of the other corrosion site. Thus, in each case the location of the corrosion sites can be easily and accurately identified, but a quantitative measure of the corrosion rate at each site becomes difficult.

APPLICATIONS

Pitting Corrosion

Pitting corrosion is a highly localized form of corrosion attack of passive metal surfaces and is generally directly related to the presence of chlorides or bromides. The development of pitting is sensitive to almost all variables associated with the interface between the metal and the electrolyte. These variables include the chloride concentration, the presence of other anions which may act as pitting inhibitors, the composition of the metal, its surface preparation and history and the electrochemical potential.[24,26-31] The potential has been shown to be decisive in the initiation and propagation of pitting. If the potential is held below a critical value usually termed the 'pitting potential,' pits do not develop. If the potential rises to or above the critical range, pitting initiates and then can continue to propagate below this potential.[29] If the potential is decreased sufficiently, the pitting eventually stops, and if held at low potentials, the pits lose the high chloride concentrations and the metal surface within the pit passivates.

The pitting behavior of stainless steels was investigated by Rosenfeld and Danilov using the adjacent reference electrode technique.[24] Their measurements were carried out in a solution containing about 0.05M $FeNH_4(SO_4)_2$ and 1.0 or 0.56M NH_4Cl. They could detect pits after 30-60 secs after contact

with the solution. Initially the rates of dissolution of all the pits were similar, however, with time, some of the pits stopped corroding or showed decreased rates. Observations of the pits under the microscope showed that they were covered by a film or shielding layer resulting from the attack of the metal by chloride ions penetrating the oxide film. Destroying the shielding layer led to passivation. The authors considered the rupture of the shield assisted the diffusion of the "passivator" into the pit. The process of passivation took a relatively long time, of the order of tens of minutes, after disruption of the shield. Also, the time for deactivation of the pits increased with the size of the pits. The deactivation process was probably a result of a diffusion process, but it is not possible to separate whether it is the result of increased diffusion of the high chloride concentration from the pit or the diffusion of bulk solutions into it, since the time dependence of both processes are similar.

The currents from the pit were related to the square root of time. The current densities, therefore, decreased and assuming a hemispherical pit, the surface area varied linearily with time. This result is in agreement with work by other investigators.[26,27]

The SRET has been used to study the pitting of type 304 stainless steels in a ferric chloride solution[20,30] composed of 0.4M $FeCl_3$ and adjusted to pH 0.9.[29] The change in the number of active pits were studied as a function of time and surface preparation. On exposing the steel to the solution, the potential of the specimen increased rapidly above the pitting potential with the generation of active pits. With time, the potential of the specimen decreased as the active pits grew and the number decreased. However, small potential increase were observed when pits passivated. The active and repassivated pits

were separated using the SRET. The active pits were always covered by a film and contained a dark green solution. Fig. 10 shows a sequence of scans represented by potential surfaces for an electropolished surface at the times shown. Each peak is associated with the currents from active pits. On the first scan, initialed one minute after exposure, fourteen pits could be identified. The number of active pits decreased and only one pit was active after 26 minutes. When the final pit was subjected to a jet of solution, it repassivated. The anodic currents polarizing the cathodic reaction then ceased and the potential rose rapidly above the pitting potential and the sequence of events observed on first contacting the specimen with the chloride solution was repeated.

It was suggested that the film over the active pits was the passive oxide film originally on the metal surface that was undermined by the pitting process.[20] This possible explanation was investigated by varying the surface preparation of the stainless steel prior to pitting. The number of active pits were again studied as a function of time and a semilogarithmic plot was used to determine the half life of the pits as shown in Fig. 11. The surface preparations studied were electropolishing or abrasion and the effects of subsequent oxidation or cathodic polarization. The results were highly dependent on surface treatment. Air oxidation of electropolished surface at temperatures above 100°C for 24 hours increased the half-lives of the pits. These changes are shown in Fig. 11 which includes the variations in the number of active pits for surfaces oxidized at 110°, 165° and 240°C and with cathodically polarized electropolished surfaces. Table 1 shows the half-lives for these and other treatments.

The results were found to be consistent with the changes in the properties of the original oxide layer over the pit before it was undermined by the pitting process. The thicker the oxide, the greater was the protection afforded to the

growing pit and the longer the pits remained active. When the metal was abraded, stresses in the oxide film lead to short half-lives (< 1 sec). The half-lifes of pits on abraded surfaces was low (~ 5 min.) even after oxidation at 250°C in comparison to similarly oxidized electropolished surfaces which gave a half-life of 480 minutes.

The pitting of stainless steels during the early development of the pits was interpreted in terms of maintaining the presence of high chloride concentrations within the pit and reducing the loss of chloride by diffusion into the lower concentration bulk solution. The presence of the oxide film over the pits hampers the diffusion of chloride which build up as a result of ionic conduction. These two factors, the presence of the oxide film and the flow of chloride into the pit, suggest that improved pitting resistance of alloys may be accomplished by either reducing the rate of dissolution of the alloy in the concentrated environment within the pit, or, by changing the properties of the passive oxide layer. The ideal passive oxide film for pitting resistance would be thin, highly stressed and easily disrupted when undermined by pitting. These properties of the film contrast with those usually considered to give improved corrosion resistance.

The additions of nitrate to the ferric chloride solution inhibits pitting corrosion. The effect of nitrate was consistent with an influence on properties of the oxide film on steels.[20] At a critical concentration of 0.075 $NaNO_3$ in the ferric chloride solution, pitting was not inhibited but the pits which initiated did not propagate for more than a few minutes. It was suggested that the nitrate weakened the film which was easily disrupted when undermined and led to repassivation.

Pitting of stainless steel was also studied in sodium chloride solutions under potentiostatic condition using the SRET. The peak heights over the pitting areas were summed. The sum was found to be linearily related to the applied current. In ferric chloride solutions, the logarithm of the summed peak heights was plotted against the corrosion potential of the specimen. The slope of this plot was similar to that observed during cathodic polarization of the steel in ferric chloride inhibited with 1M $NaNO_3$ to prevent pitting. The agreement between the slopes indicated that under open circuit conditions the cathodic polarization characteristics could be determined from the variation of the potential peaks since they are a measure of the polarizing current.[20]

Gainer and Wallwork[23] used the rotating cylinders to study the effects of surface abrasion and metallurgical features on the pitting corrosion of mild steels in 10^{-5}N NaCl. The potential variation caused by difference in current flow, were greatest for coarse abrasion on 280 grit paper. A 600 grit and < 1μ diamond paste finishes gave similar results with smaller potential fluctuations. The differences observed on the coarsely abraded surface indicate a high density of active pits ($\sim 2.5 \times 10^3/cm^2$) and their activity was probably associated with the greater true cathodic area available on the rougher surface. The number of active sites decreased with time and the intensity of corrosion of the remaining active sites increased. The formation of pits around active sites were found to be related to presence of inclusions and scratches.

Intergranular Corrosion

Intergranular corrosion (IC) is defined as the localized attack, in certain corrosive media, at the grain boundaries of steels. This form of corrosion is particularly severe in stainless steels which are sensitized. In austenitic stainless steels, sensitization is caused by (1) heat treating the

alloy in the temperature range of 500-850°C for a few hours and quenching; (2) cooling slowly through the above mentioned temperature range and; (3) welding.[32,33] It is generally believed that sensitization leads to the precipitation of chromium rich carbides at the grain boundaries and the depletion of chromium adjacent to the boundary.[34] This depletion has been observed by scanning transmission electron microscopy.[35] The depletion of chromium at the grain boundary leads to IC of stainless steels in certain environments.

The SRET has been used to determine the accelerated corrosion of grain boundary region in sensitized type 304 stainless steel. Fig. 12(a) is a potential scan during the IC of a large grain size (diameter $\sim$ 3 mm), sensitized (600°C for 24 h) type 304 stainless steel in 2.5N H_2SO_4 at room temperature at a potential of -200 mV vs. SCE. Fig. 12(b) is a line drawing of the etched boundaries on metallographic observation after the test showing a clear relation between the etched boundaries (dark lines) and the peak maximum in Fig. 13(a) (dotted lines). The potential peaks in Fig. 13(a) were observed only in the case of sensitized type 304 stainless steel, while solution annealed (1100°C for 3 hrs) samples exhibited no potential peaks and no grain boundary etching in this solution.

The dependence of intergranular corrosion on the electrochemical potential of type 304SS in 2.5N H_2SO_4 can be determined by slowly increasing the potential (0.3 V/h) of the sample in the anodic direction and scanning the surface simultaneously. In the potential region where sensitized type 304SS is susceptible to IC, peaks are observed on scanning, while in the potential region, where the material does not undergo IC no peaks are observed. This is shown schematically in Fig. 13. The material is susceptible to IC between -280 mV to +80 mV vs. SCE and then again in the transpassive region (> 820 mV vs. SCE).

This result is consistent with the observation of IC of this steel in the Strauss test and the nitric acid test.[36]

In order to obtain a semi-quantitative relation between the corrosion current flowing and the resulting potential field in the electrolyte due to intergranular corrosion, experiments were run in 1N H_2SO_4 + 0.05M KCNS using the back scan procedure.[36,37] The sample is held at -500mV in the electrolyte for 5 mins., and then instantaneously raised to +200mV. The sample is cathodic at -500mV and passive at +200mV (vs. SCE). The sample is held at +200mV for 2 mins., and then decreased in the reverse direction from +200mV to -500mV at a rate of 3V/hr. In case of solution annealed samples, the surface was passive to -100mV, when the currents became cathodic. However, in the case of sensitized samples large anodic currents are observed and at -100mV the polarization curve showed an anodic peak. The anodic peak is a result of the active dissolution of the sensitized grain boundaries.

Fig. 14 shows a polarization curve for type 304SS sensitized at 600°C for 40 h, obtained by the back scan technique. In the potential region, -380mV to -30mV, an active peak is observed. In this region, increased grain boundary dissolution takes place. This is presented as potential peaks in Fig. 15. The peak height of one of the peaks is plotted against the applied potential in Fig. 14. It is observed that the shape of the peak height versus the current density curve is similar to the potential versus the current density curve. This demonstrates that the active current flow from the grain boundaries of the sensitized stainless steel, and the peak height is proportional to the total current. Also, that there is a direct correlation between the current and peak height. In the case of solution annealed samples no anodic corrosion current was observed, nor were any potential peaks measured.

Grubitsch and Zirkl[38] have used the SRET to determine IC in precipitation hardened aluminum-copper alloys. On heat treatment at 150°C for 1 hr., $CuAl_2$ is precipitated at the grain boundaries of the alloy and this results in a precipate free zone adjacent to it. The grain boundary region is preferentially attached in a large number of chloride containing acidic solutions. However, when the alloy is solution treated (500°C for 12 hr.), i.e. no precipitation or the copper free zone is formed, it is not susceptible to IC.

Welds

In welding, it is assumed that corrosion behavior of the weld metal and the parent metal is similar. However, this is not always the case, particularly when austenitic stainless steels are considered. The weldment, i.e. the weld metal and the adjacent parent metal affected by the heat of the welding, may be susceptible to varying degrees of preferential attack. The weld metal may corrode more or less than the parent metal due to differences in composition or metallurgical condition.[33] In addition, the base metal heated during the welding may corrode as a result of metallurgical changes caused by heating cycles.[32] The factors that can influence the type and degree of preferential attack depend on 1) composition and structure of base and weld metal, 2) metallurgical changes in the parent metal due to welding 3) welding process and procedure 4) size of material welded and 5) the type of the environment.[40]

The SRET has been successfully used to identify the preferential attack of type 304 stainless steel weldments. The type of preferential attack observed are 1) attack of the ferrite in the weld matrix 2) fusion boundary corrosion 3) intergranular corrosion of the sensitized material in the heat-affected zone of the base metal. Fig. 16 shows the potential peaks measured on type 304

stainless steel weldment, prepared by manual shielded arc gas welding type 308 weld metal, in 2.5N H_2SO_4 at room temperature at various potentials. The weldment was slowly polarized (0.3V/hr) in the anodic direction from -500mV to + 1V vs. SCE, and simultaneously, the microtip reference electrode was scanned over the face of weldment. The potential regions exhibiting the different types of preferential attacks are shown in Fig. 17.

At more negative potentials, where the sample is cathodic, the weld material exhibits larger cathodic current densities than the parent metal. However, at a potential of -420mV, where the overall current is cathodic, the weld exhibits preferential anodic dissolution, Fig. 16. The preferential attack of the weld extends into the anodic region and the rate of attack increases with increase in anodic current. The preferential attack of the weld stops when the metal is passivated. However, in the transpassive region, the weld again corrodes preferentially and the rate of attack increases with increase in the current.

At, and close to the maximum in the anodic peak, the fusion boundary is preferentially attacked. The preferential corrosion of the fusion boundary is shown as large peaks at the ends of the broad peak produced by corrosion of the weld, as shown in Fig. 16 for applied potentials -330, -300 and -250 mV vs. SCE. As the sample passivates and the total current of the sample decreases, the corrosion of the fusion boundary decreases drastically.

In Fig. 16, at an applied potential of -250 to -40 mV vs. SCE, the development of a peak in the base metal is observed. This peak is due to the intergranular attack of the sensitized zone. The peak increases as the polarization current decreases, i.e. the metal is passivated. The single, large peak is a result of the preferential corrosion of a large number of grain boundaries in

the sensitized zone. The peak is observed from -310mV to +100mV, beyond which the complete weldment is passivated. The position of this maximum changes with potential. This results from changes in position of the most susceptible regions in the sensitized zone, with potential.

Micrographs of the attacked regions we obtained in order to determine the effect of the local microstructure on the various modes of preferential attack, Fig. 18. In the weld center, the microstructure consists of a network of ferrite platelets in an austenitic matrix. In the active region, the increased corrosion of the ferrite gives rise to the potential peak. It is known that ferrite is more active than austenite at the lower potential.[41,42] The corrosion of the ferrite gives rise to the anodic peak of the weld although the total current of the sample is cathodic. The waves on the peak of the weld corrosion is due to the presence of the root of the run in the weld. At the fusion boundary, the ferrite is not in the form of fine platelets, but is present as large, separate particles. This increased ferrite content at the boundary gives rise to the enhanced corrosion of the fusion boundary. No sigma phase was observed at the fusion boundary. On each side of the weld, the parent material is in the solution annealed state and no grain boundary etching was observed. At a distance of 2mm to 3mm from the weld fusion line, the grain boundaries are etched. This increased corrosion from the sensitized grain boundaries gives rise to the broad peak over this region.

Similar differences in the corrosion of the weld and the parent metal have been observed for ferritic 17% Cr steels in chloride containing solutions.[39] It has been found that the type of preferential attack depends on the impressed applied current and the electrolyte, for example, the chloride concentration, pH and the presence of organic solvents. Hildebrand and Schwenk[14] have measured

the increased anodic activity in the heat affected zones of austenitic stainless steel welds. Using a SRET, they were able to plot the potential field arising from corrosion of the sensitized region in heat affected zones in 10^{-3}N alcoholic HCl.

Sensitization in the heat affected zone adjacent to the weld is probably the most common cause of intergranular corrosion and intergranular stress corrosion cracking in stainless steels in service. In order to determine the susceptibility of a given weldment to these forms of localized attack, it is necessary to develop a test which will give 1) the location of the sensitized zone, and 2) a quantitative measure of the degree of sensitization. The SRET meets the above mentioned requirements and has been successfully used to give the location and the degree of sensitization of the weldments for various welding process variables. The details of the test are given in detail elsewhere.[21] In summary, the test consists of scanning across the weldment while it is polarized by the back scan technique (described earlier). A representative scan for type 304SS weldment over the heat affected zone is shown in Fig. 19. The location and width of potential peak gives an indication of the location and width of the sensitized zone as observed in the etched sample in Fig. 19, and the peak height is proportional to the degree of sensitization. This technique is more sensitive than accepted chemical methods of evaluating stainless steel welds for their resistance to intergranular corrosion.

Stress Corrosion Cracking

Stress corrosion cracking in metal systems is concerned with the nucleation and propagation of cracks in stressed metals induced by the environment. In order to understand the mechanism of cracking in any particular metal-environment system, it is necessary to determine the electrochemical

reaction(s) that take place at the crack tip. The SRET provides an ideal system to study this reaction and in this section, an example is given of SCC of type 304 stainless steel in a chloride solution.

The electrochemical cell around the sample is shown in Fig. 21. A tensile specimen with a 90° notch having a radius of about 125 μm at the tip was inserted through slits in a thin walled fluorinated container. The specimen was sealed to the container with silicon rubber. The sample was loaded horizontally in a tensile machine to an initial stress of 8.5 Ksi. The upper face of the specimen with the "V" notch was metallographically polished and all but part of this surface around the notch was coated with the silicon rubber. The electrolyte used was 20 molal LiCl controlled at 90°C using an infra-red lamp.

Following the initial exposure to the electrolyte pitting was observed optically. The progress of large pits which remained active was monitored using the SRET. After some time, the intensity of the pitting decreased and the potential of the specimen rose. When the pitting stopped, potential peaks were observed at the root of the notch associated with the initial stages of cracking. Fig. 22 shows the potential peaks observed after the cracking had progressed into the metal. The propagation of the potential peaks was studied. Fig. 23 gives the magnitude of potential peaks along the length of the crack at various times taken from figures similar to Fig. 22. The shape of these plots which are non-symetrical, indicates that although the dissolution rate was greatest at the crack tip, the entire crack remained active. These observations are consistent with most theories of stress corrosion cracking, i.e. rapid dissolution takes place at the high stress intensity at the crack tip where fresh metal is continuously exposed to the corrosive environment.[43] However, the persistent anodic dissolution of the crack surfaces shown using SRET, during cracking and after

the specimens fail, is in conflict with models which suggest that the crack surface must passivate to account for crack propagation. The SRET suggests that the exposed metal remains active but with decreased dissolution rates. The theory based on the rupture of passivating oxide layers appears to be a simplification of the process. The detailed theory would require to take into account rupture of a more complex corrosion product or other processes, such as stress stimulated dissolution at the crack tip, to be consistent with these observations.

SUMMARY

The SRET has been shown to offer a technique for studying localized forms of corrosion including pitting, intergranular corrosion and stress corrosion cracking. These processes are associated with relatively rapid dissolution rates and observable potential variation in solution. The technique is also useful in separating preferential dissolution or cathodic reactions under controlled potentials where external currents flow.

Other electrochemical measurements e.g. polarization techniques, can give detailed information about processes under study, but, difficulties arise in the complete separation of the anodic and cathodic areas and duplicating the conditions operative during corrosion. The SRET overcomes these difficulties, and offers an approach for *in situ* determination of the corrosion processes and allows for clarification of the factors involved, without extraneous effects influencing the corrosion.

TABLE 1 Variations of Pit Half-life with Surface Preparation

Surface treatment	Pit half-life,* min
Electropolished and cathodically polarized	<1
As electropolished	22
Electropolished and oxidized at 110°C for 24 hr	90
Electropolished and oxidized at 165°C for 24 hr	150
Electropolished and oxidized at 240°C for 24 hr	430
Electropolished and oxidized at 250°C for 2 hr	480
Electropolished and oxidized at 300°C for 22 hr	340
Electropolished and oxidized at 375°C for 2 hr	270
Abraded with 600 grade SiC	<1
Abraded and oxidized at 250°C for 8 hr	5

*Maximum variation of 20%

REFERENCES

1. Localized Corrosion - Cause of Metal Failure ASTM, STP 516, American Society of Testing & Materials, 1972.
2. Brown, B.F., Kruger, J. and Staehle, R.W., Eds., Localized Corrosion, National Association of Corrosion Engineers, 1974.
3. Evans, U.R. and Hoau, T.P., Proceedings of the Royal Society A, Vol. 137, 1932, p. 343.
4. Compton, K.G. and Turley J.A., Galvanic and Pitting Corrosion - Field and Laboratory Studies, ASTM STP 576, American Society for Testing and Materials, 1976, p. 56.
5. Coriou, H., Monnier A., Pinard-Legry, G. and Plante, G., in Ref. 1, p. 368.
6. Baboian, R., in Electrochemical Techniques for Corrosion, National Association of Corrosion Engineers, 1977, p. 73.
7. Lajain, H. Z.F. Werkstofftechnik, Vol. 2 (1971), p. 19.
8. Lajain, H. Werkstoffe und Korrosian, Vol. 23 (1972), p. 537.
9. Evans, U.R. and Agar, J.N., see Evans, U.R., The Corrosion and Oxidation of Metals, Edward Arnold Ltd., 1960, p. 862; Evans, U.R., Journal of the Iron and Steel Institute, I, Vol. 141, 1940, p. 219.
10. Jaenicke, W., Z. Physik Chem., Vol. A191, 1943, p. 350.
11. Jaenike W. and Bonhoeffer, K.F., Z. Physik Chem., Vol. 193, 1944, p. 301.
12. Copson, H.R., Journal of the Electrochemical Society, Vol. 84, 1943, p. 71.
13. Rozenfeld, I.L. Atmospheric Corrosion of Metals, National Association of Corrosion Engineers, 1972, p. 83.

14. Hildebrand, H. and Schwenk, W., Werkstaffe und Korrosion, Vol. 23, 1972, p. 364.

15. McCafferty, E., Journal of the Electrochemical Society, Vol. 124, 1977, p. 1869.

16. Smyol, W.M. and Newman, J., Journal of the Electrochemical Society, Vol. 123, 1976, p. 1423.

17. Waber, J.T., Corrosion, Vol. 13, 1957, p. 95t.

18. Waber, J.T. and Rosenbloth, M., Journal of the Electrochemical Society, Vol. 102, 1955, p. 344.

19. Wagner, C., Journal of the Electrochemical Society, Vol. 98, 1951, p. 116.

20. Isaacs, H.S., in Ref. 1, p. 158.

21. Vyas, B. and Isaacs, H.S., Intergranular Corrosion of Stainless Alloys, ASTM, STP 656, R.F. Steigerwald, Ed., American Society for Testing and Materials, 1978, p. 133.

22. Bhansali, J.J. and Hepworth, M.T., Journal of Physics E. Scientific Instruments, Vol. 7, 1974, p. 681.

23. Gainer, L.J. and Wallwork, G.R., Corrosion, Vol. 35, 1979, p. 61.

24. Rosenfeld, I.L. and Danilou, I.S., Corrosion Science, Vol. 7, 1967, p. 129.

25. Eyring, H.J., Physical Chemistry, Vol. 9A, 1970, p. 359.

26. Engell, H.J. and Stolica, N.D., Z. Phys. Chem., Vol. 20, 1959, p. 113.

27. Sato, N., Nakagawa, T., Kudo, K. and Sakashita, M.S. in Ref. 1 p. 447.

28. Isaacs, H.S. and Kissel, G., Journal of the Electrochemical Society, Vol. 119, 1972, p. 1628.

29. Wilde, B.E. and Williams, E., Journal of the Electrochemical Society, Vol. 117, 1970, p. 775.

30. Galvele, J.R., in Passivity of Metals, R.P. Frankenthal and J. Kruger, Eds., The Electrochemical Society Inc., 1978, p. 285.

31. Wilde, B.E. and Williams, E., Electrochimica Acta, Vol. 16, 1971, p. 1971.

32. Cowan, R.L. and Tedmon, Jr., C.S., Advances in Corrosion Science and Technology, Vol. 3, 1973, p. 293.

33. Henthorne, M., Localized Corrosion - Cause of Metal Failure, ASTM, STP 516, 1972, p. 66.

34. Tedmon, Jr., C.S., Vermilyea, D.A. and Rosolowski, J.H., J. Electrochem. Soc., Vol. 118, 1971, p. 192.

35. Pande, C.S., Suenaga, M., Vyas, B., Isaacs, H.S., and Harring, D.F., Scripta Met., Vol. 11, 1977, p. 601.

36. ASTM Designation, Recommended Practice for Detecting Susceptibility to Intergranular Attack in Stainless Steel, 1970.

37. Novak, P., Steppe, R. and Franz, F., Corrosion, Vol. 31, 1975, p. 344.

38. Clarke, W.L., Cowan, R.L. and Walker, W.L., Intergranular Corrosion of Stainless Alloys, ASTM, STP 656, R.F. Steigerwald, Ed., American Society for Testing and Materials, 1978, p. 99.

39. Grubitsch, H. and Zirkl, A., Werkstoffe und Korrosion, Vol. 23, 1972, p. 565.

40. Brautigam, F.C., Corrosion, Vol. 31, 1975, p. 101.

41. Gooch, T.C., Honeycombe, J. and Walker, P., Br. Corrosion J., Vol. 6, 1971, p. 148.

42. Cihal, V. and Prazak, M.J., Iron Steel Inst., Vol. 193, 1959, p. 360.

43. Latanision, R.M. and Staehle, R.W., in Fundamental Aspects of Stress Corrosion Cracking, R.W. Staehle, A.J. Forty and D. van Rooyen, Eds., National Association of Corrosion Engineers, 1969, p. 278.

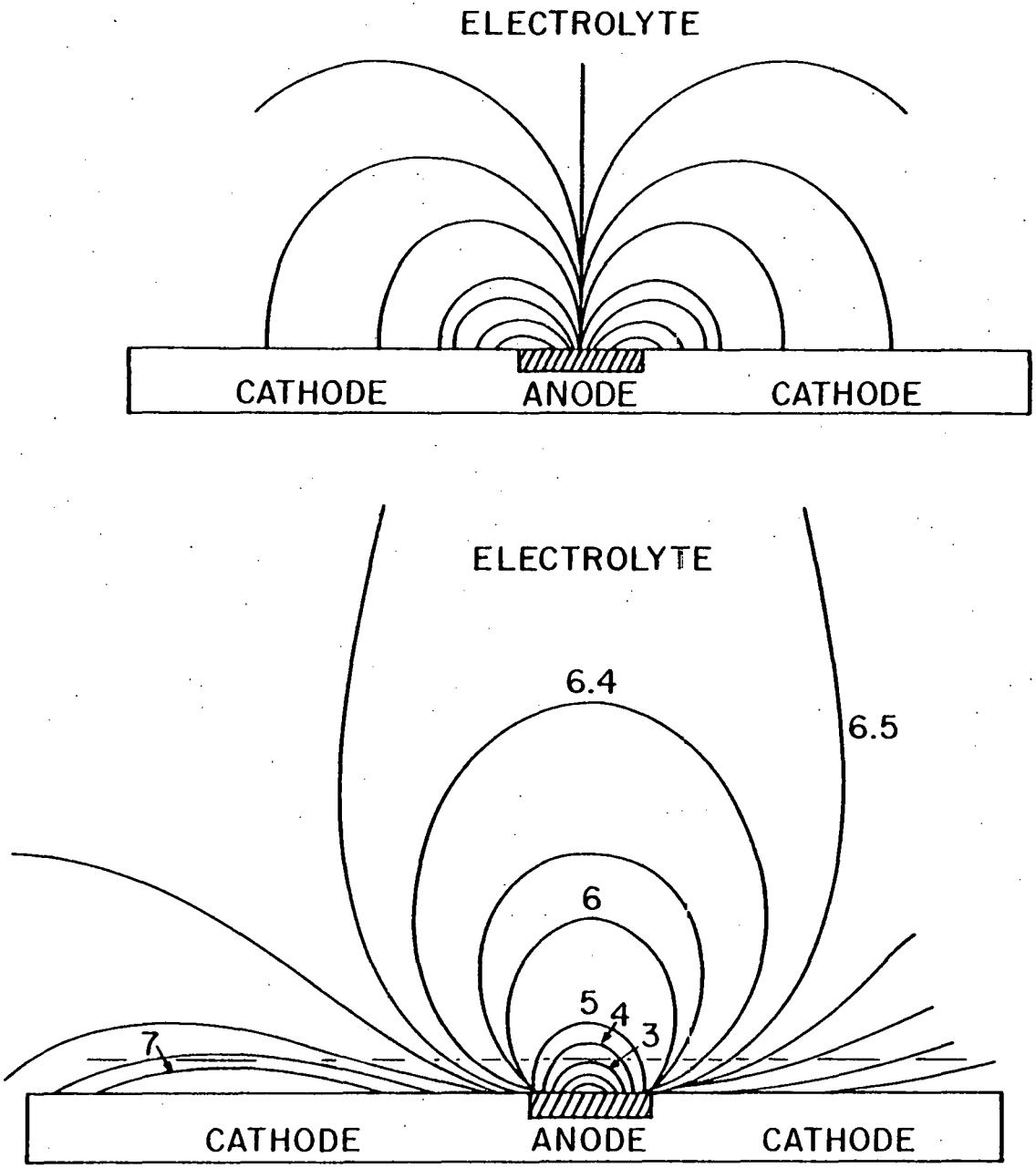
ELECTROLYTE
CATHODE
ANODE
CATHODE
ELECTROLYTE
6.4
6.5
6
5
4
3
7
CATHODE
ANODE
CATHODE

FIG. 1

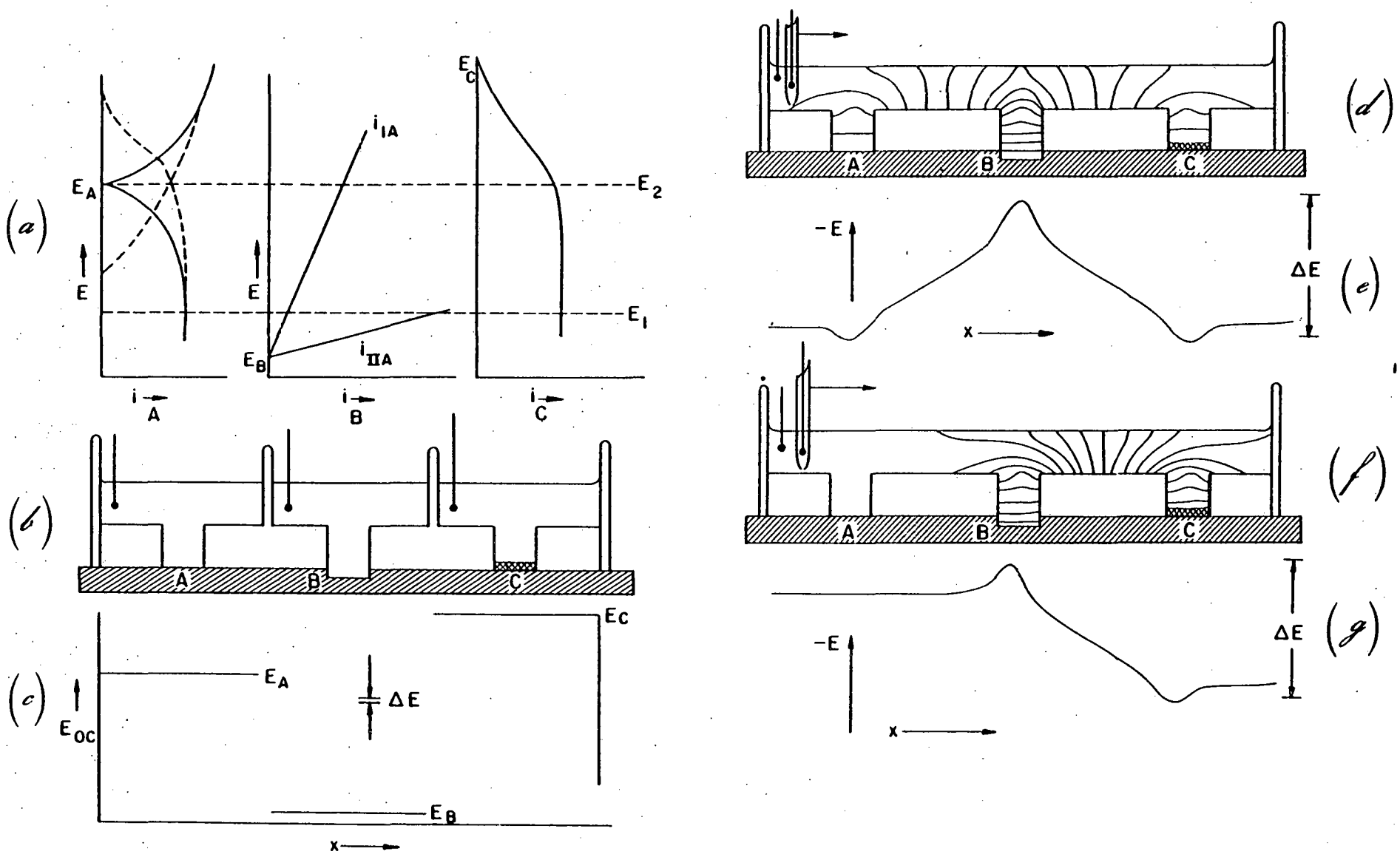
(a)
E_A
E_2
E_1
E_B
E_C
E
i_{IA}
i_{IIA}
i
A
B
C
(b)
A
B
C
(c)
E_A
E_{OC}
E_C
E_B
ΔE
x
(d)
A
B
C
(e)
-E
x
ΔE
(f)
A
B
C
(g)
-E
x
ΔE

FIG. 2

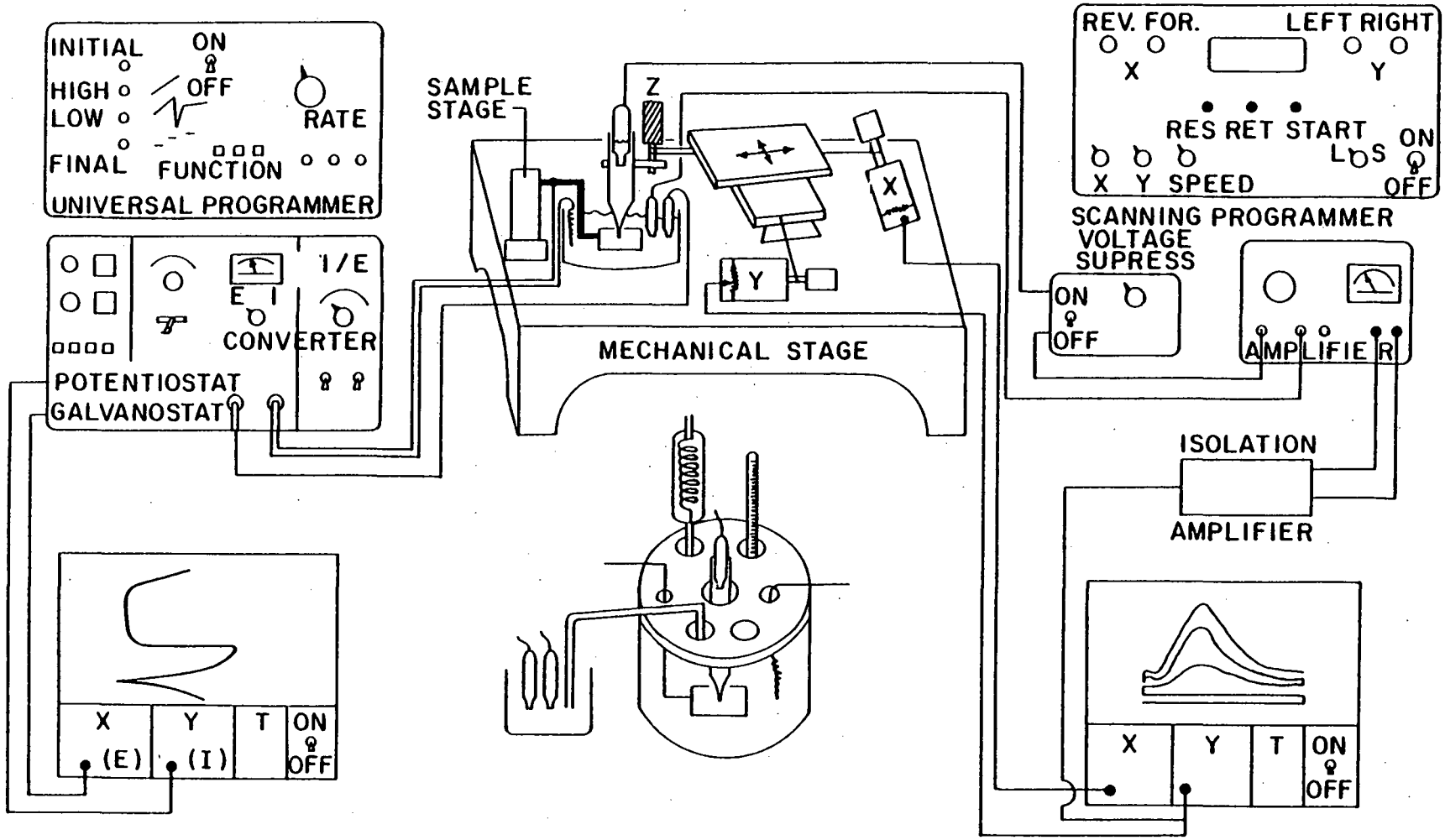
INITIAL
ON
HIGH
OFF
LOW
RATE
FINAL
FUNCTION
UNIVERSAL PROGRAMMER
I/E
E I
CONVERTER
POTENTIOSTAT
GALVANOSTAT
SAMPLE STAGE
Z
X
Y
MECHANICAL STAGE
REV. FOR.
LEFT RIGHT
X
Y
RES RET START
ON
LOS
X Y SPEED
OFF
SCANNING PROGRAMMER
VOLTAGE SUPRESS
ON
OFF
AMPLIFIER
ISOLATION
AMPLIFIER
X
Y
T
ON
OFF
(E)
(I)

FIG. 3

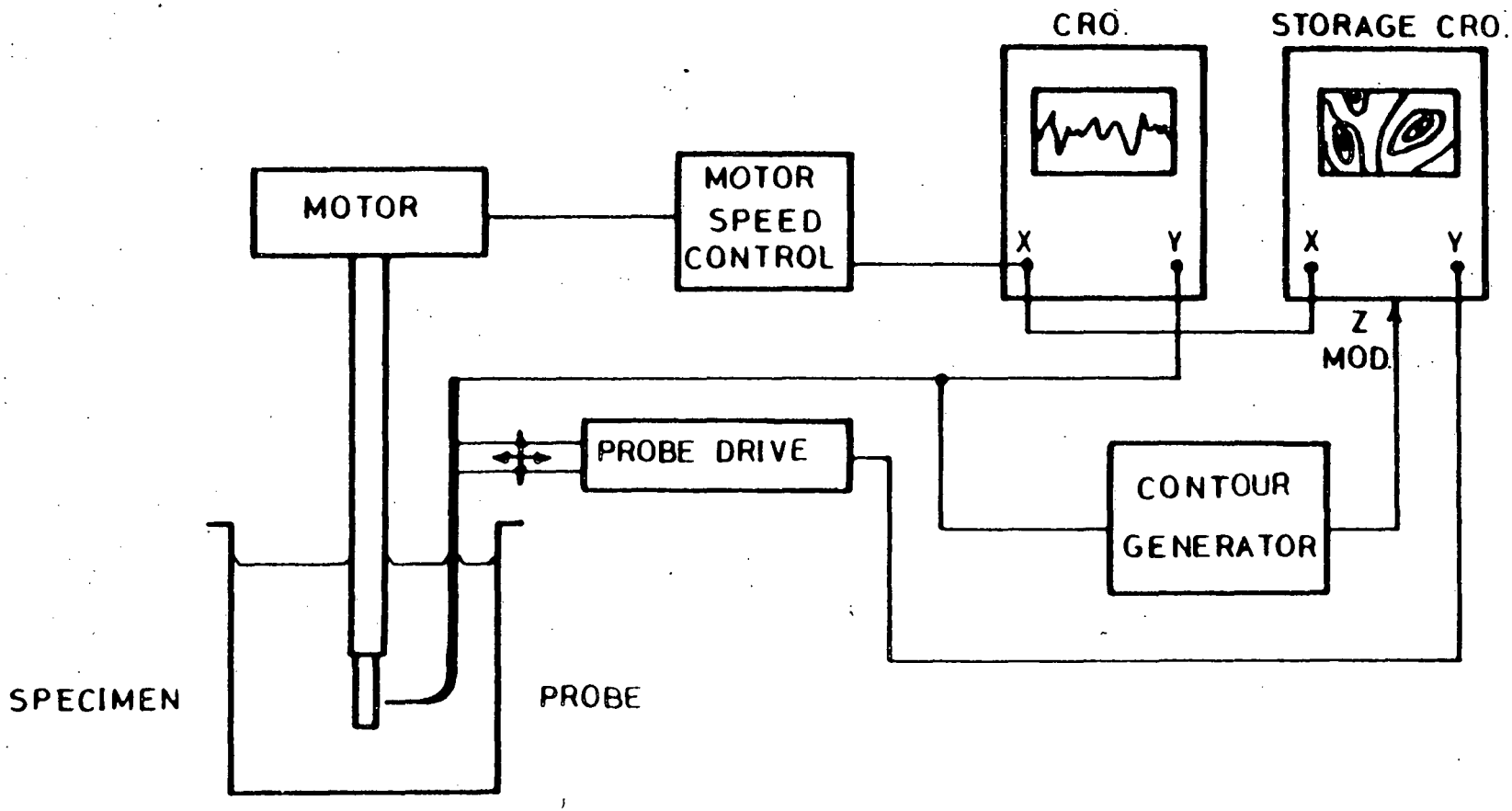
CRO.
STORAGE CRO.
MOTOR
MOTOR SPEED CONTROL
X
Y
X
Y
Z MOD.
PROBE DRIVE
CONTOUR GENERATOR
SPECIMEN
PROBE

FIG. 4

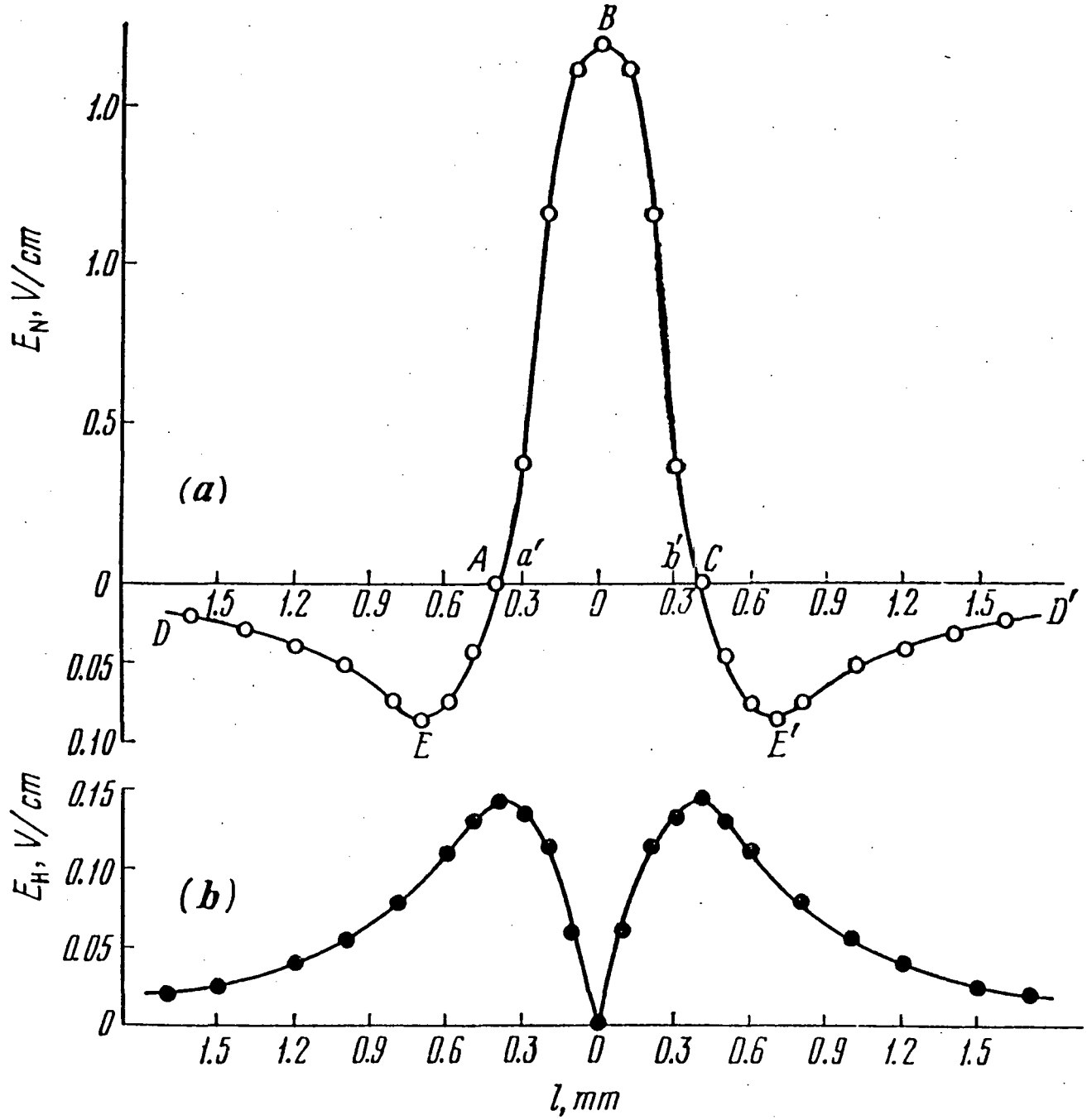
B
1.0
1.0
0.5
E_N, V/cm
(a)
A
a′
b′
C
0
1.5
1.2
0.9
0.6
0.3
0
0.3
0.6
0.9
1.2
1.5
D
D′
0.05
0.10
E
E′
0.15
0.10
0.05
0
E_H, V/cm
(b)
1.5
1.2
0.9
0.6
0.3
0
0.3
0.6
0.9
1.2
1.5
l, mm

FIG. 5

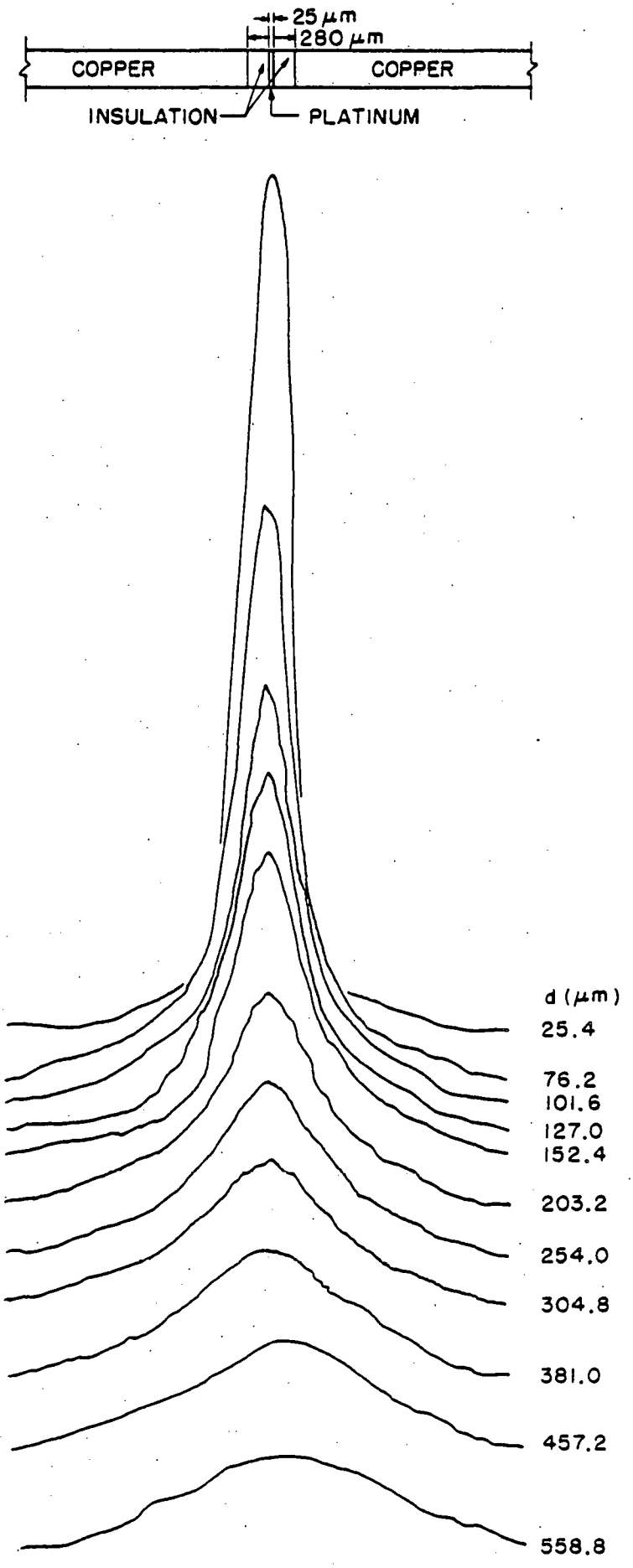
25 μm
280 μm
COPPER
COPPER
INSULATION
PLATINUM
d (μm)
25.4
76.2
101.6
127.0
152.4
203.2
254.0
304.8
381.0
457.2
558.8

FIG. 6

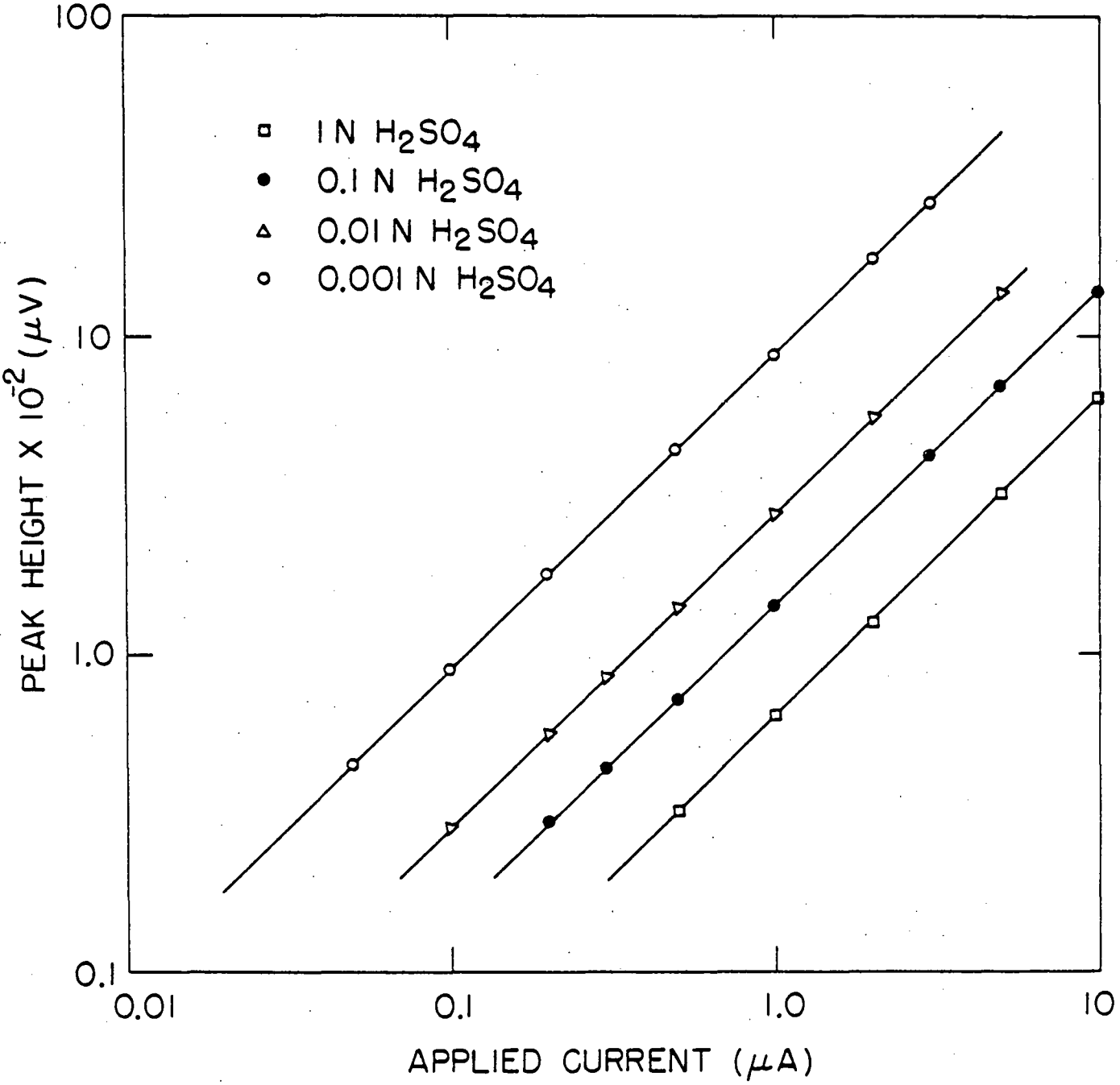
100
10
1.0
0.1
0.01
0.1
1.0
10
PEAK HEIGHT X 10^{-2} (μV)
APPLIED CURRENT (μA)
1 N H_2SO_4
0.1 N H_2SO_4
0.01 N H_2SO_4
0.001 N H_2SO_4

FIG. 7

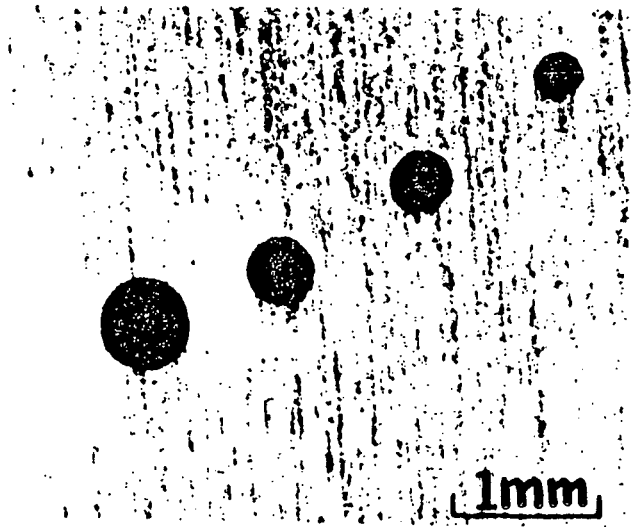

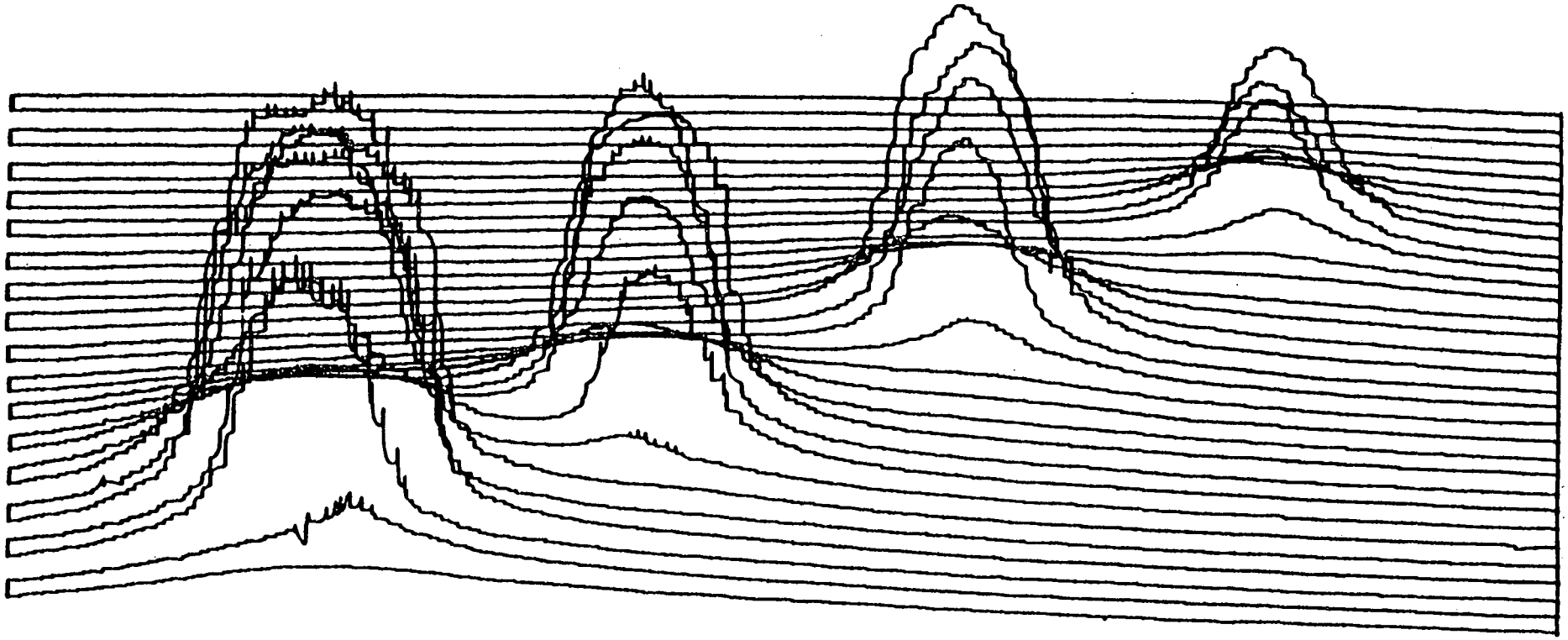

FIG. 8

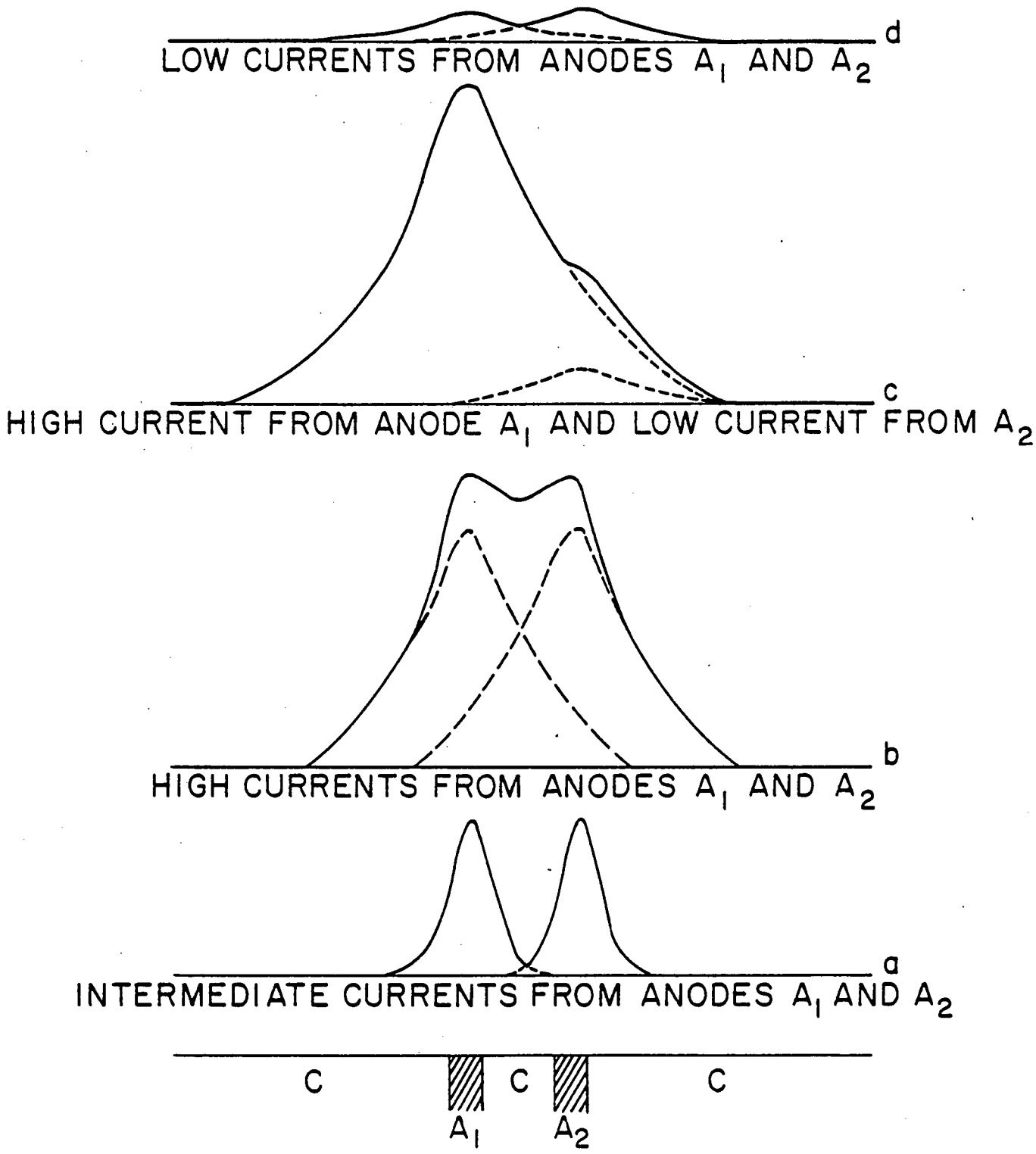
d
LOW CURRENTS FROM ANODES A1 AND A2
c
HIGH CURRENT FROM ANODE A1 AND LOW CURRENT FROM A2
b
HIGH CURRENTS FROM ANODES A1 AND A2
a
INTERMEDIATE CURRENTS FROM ANODES A1 AND A2
C
C
C
A1
A2

FIG. 9

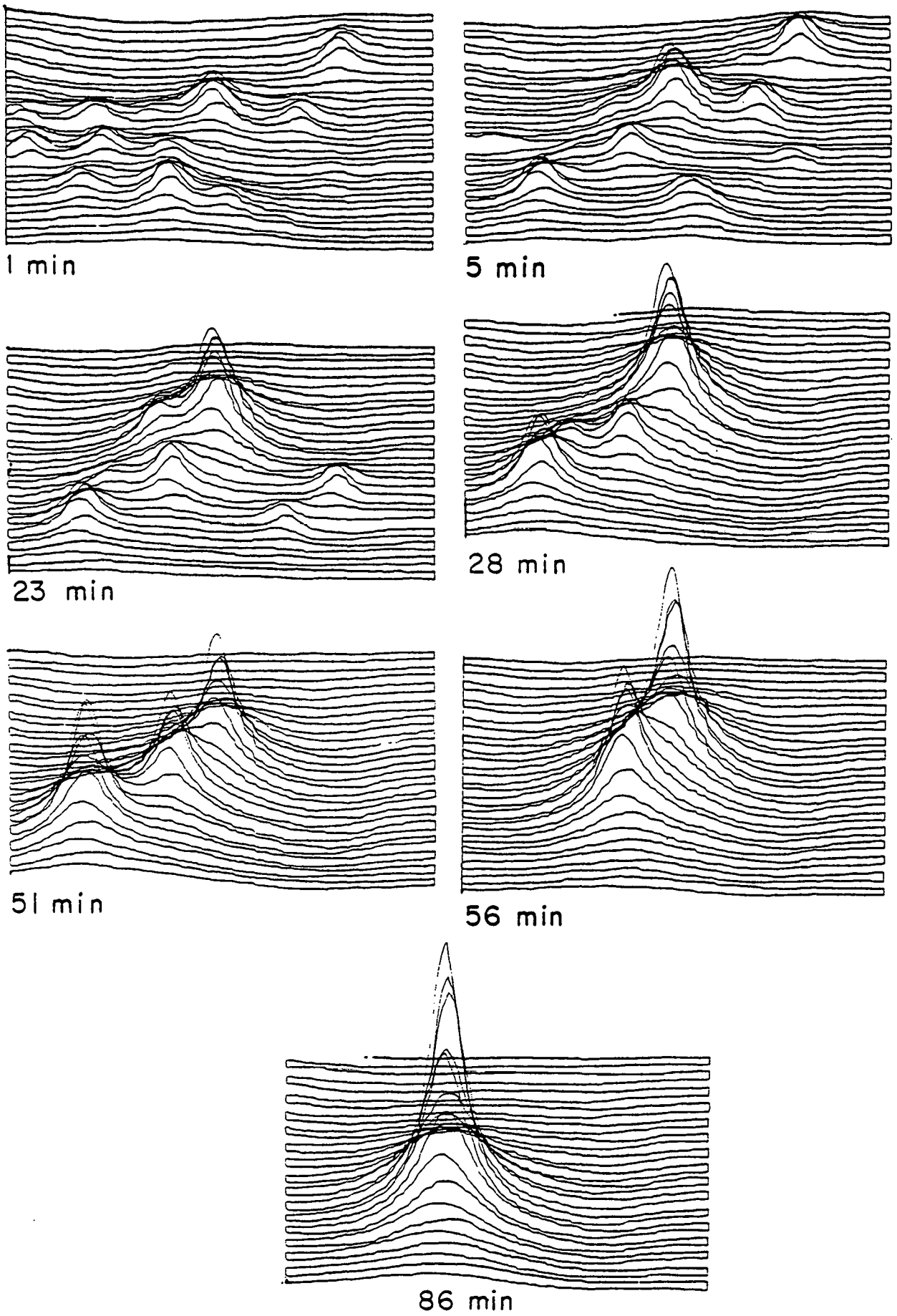

FIG. 10

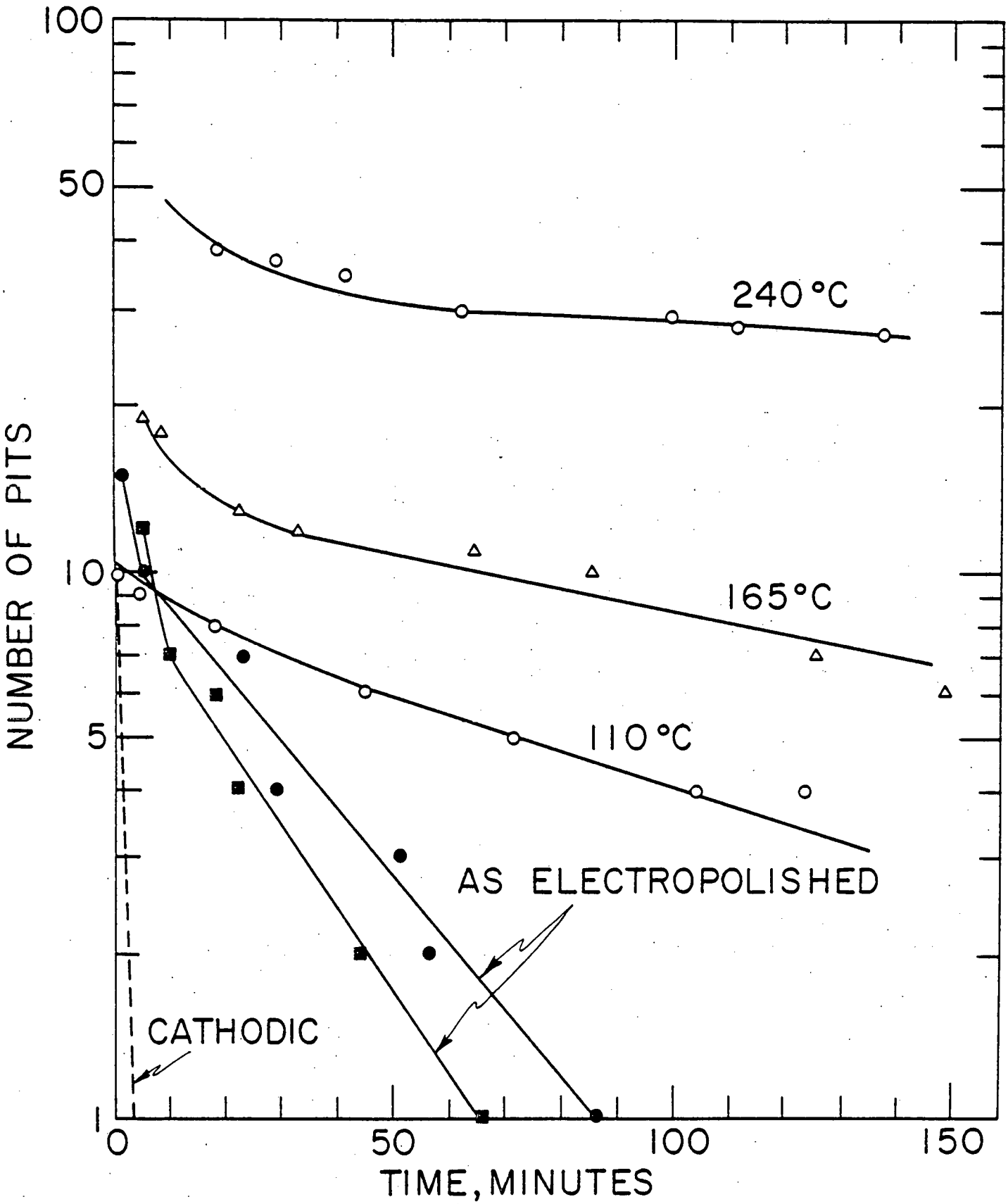
100
50
10
5
1
NUMBER OF PITS
240°C
165°C
110°C
AS ELECTROPOLISHED
CATHODIC
0
50
100
150
TIME, MINUTES

FIG. 11

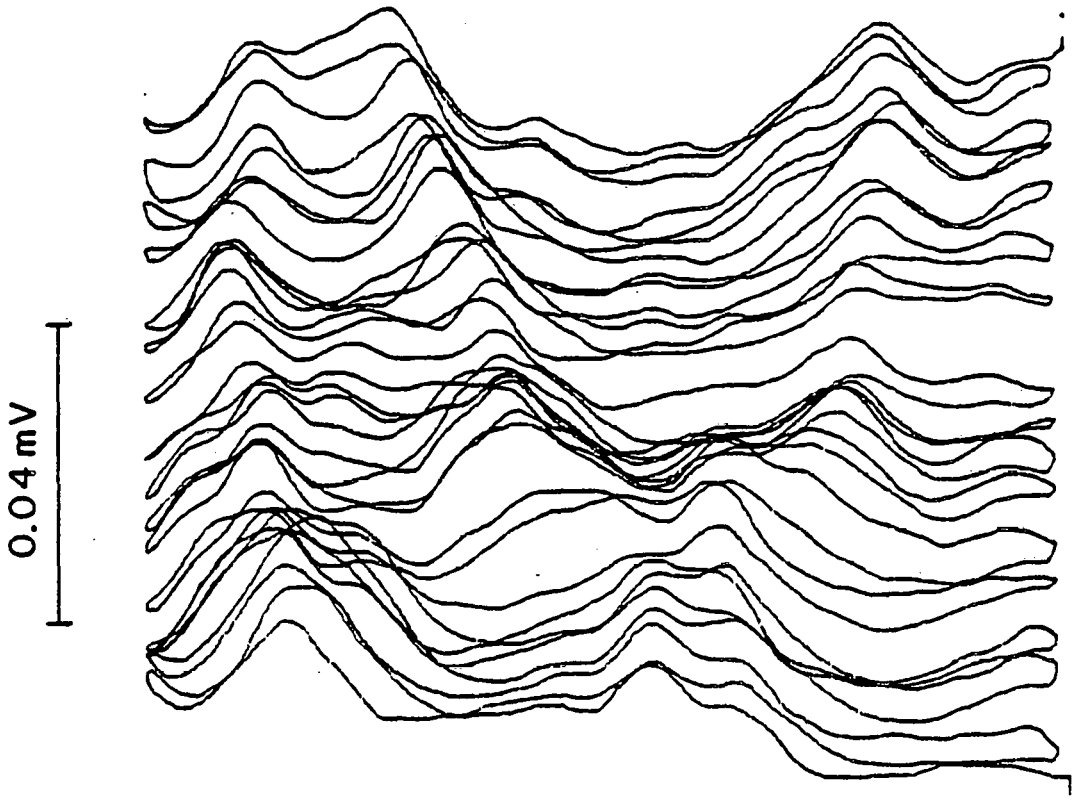

(A)

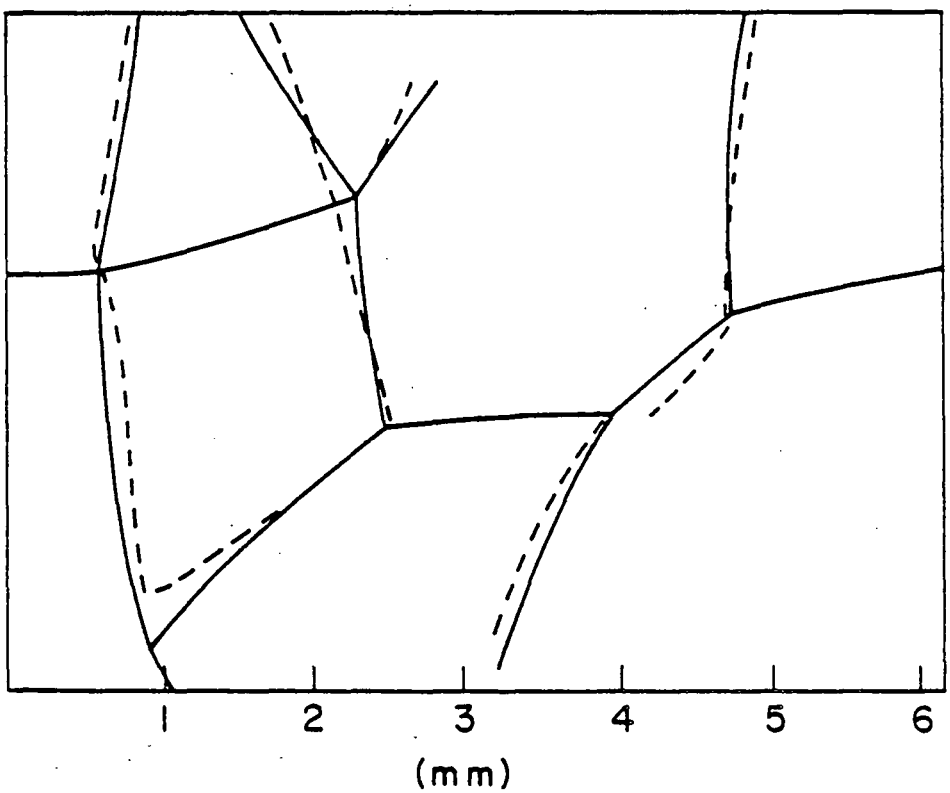

(B)

FIG. 12

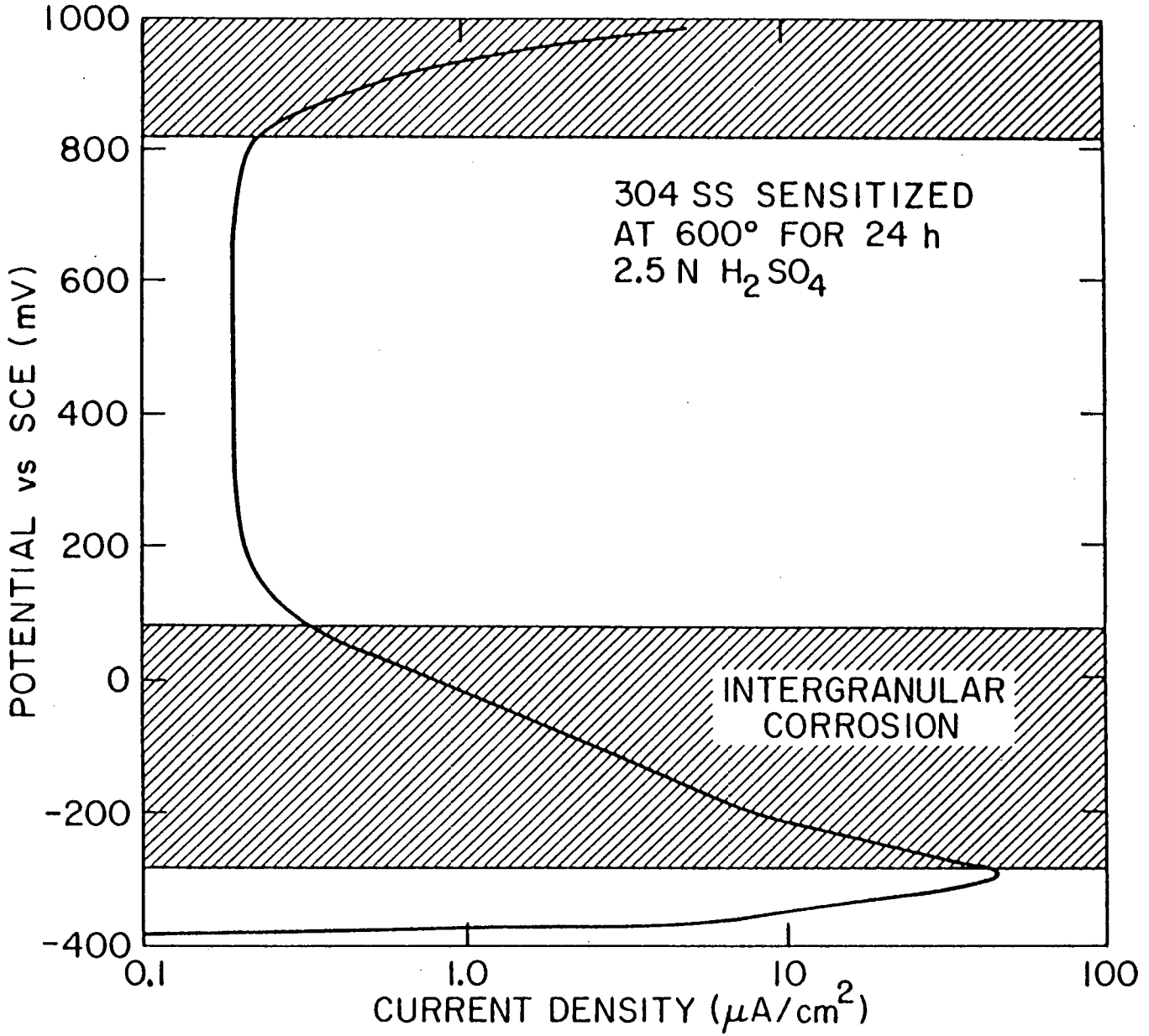
1000
800
600
400
200
0
-200
-400
POTENTIAL vs SCE (mV)
304 SS SENSITIZED
AT 600° FOR 24 h
2.5 N H_2SO_4
INTERGRANULAR
CORROSION
0.1
1.0
10
100
CURRENT DENSITY ($\mu A/cm^2$)

FIG. 13

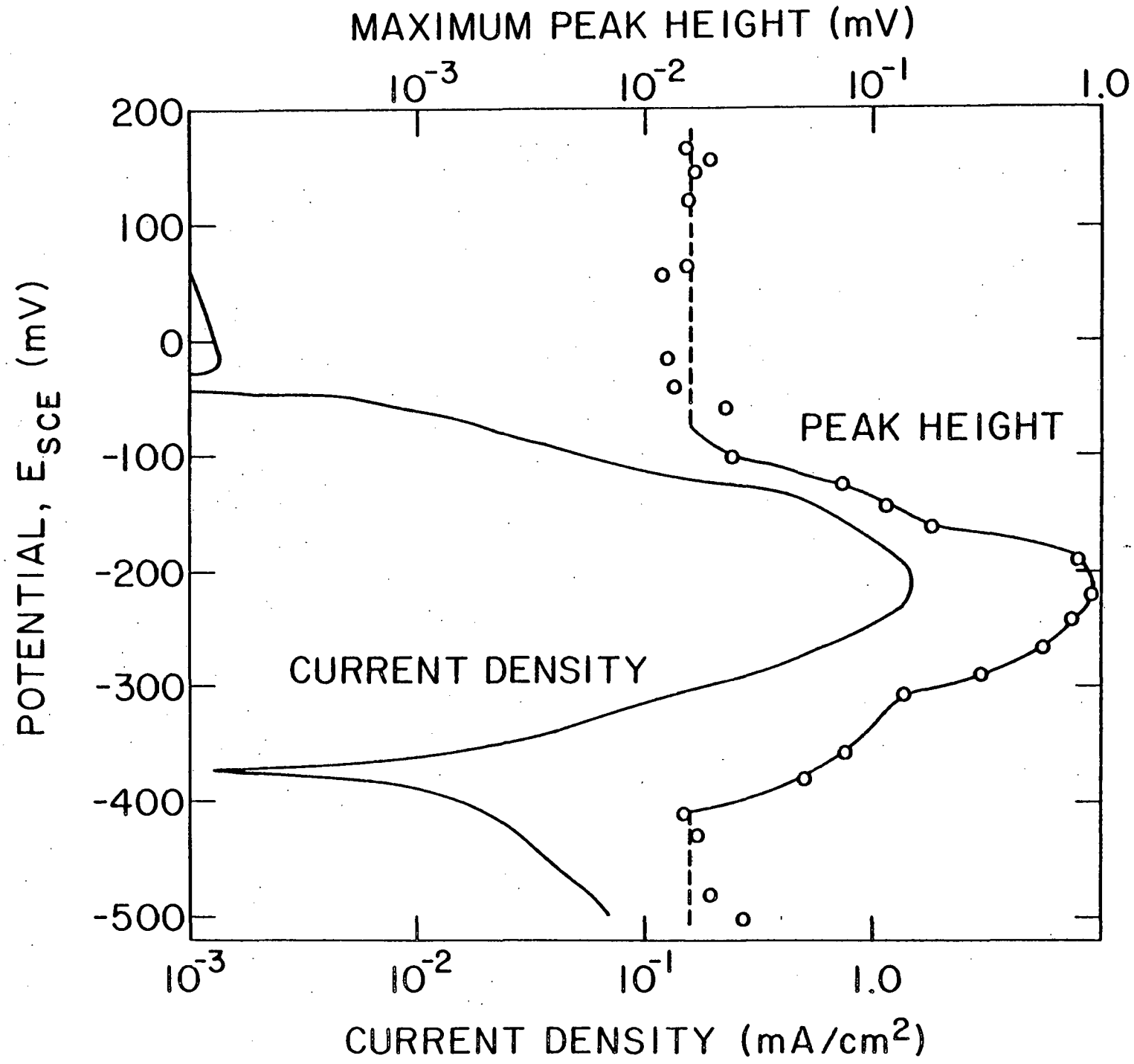
MAXIMUM PEAK HEIGHT (mV)
10^{-3}
10^{-2}
10^{-1}
1.0
200
100
0
-100
-200
-300
-400
-500
POTENTIAL, E_{SCE} (mV)
PEAK HEIGHT
CURRENT DENSITY
10^{-3}
10^{-2}
10^{-1}
1.0
CURRENT DENSITY (mA/cm^2)

FIG. 14

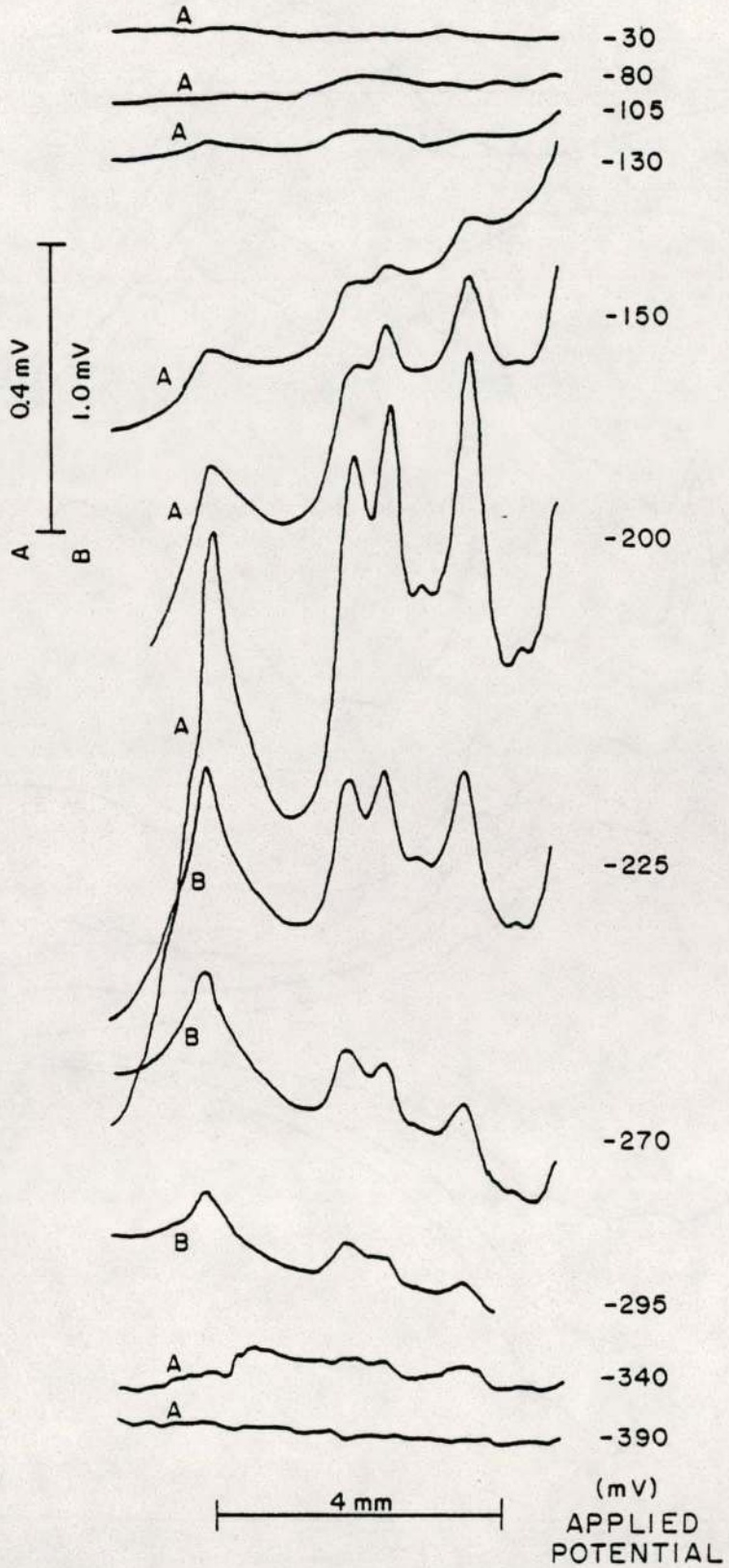
A
-30
A
-80
A
-105
-130
0.4 mV
1.0 mV
A
B
-150
A
-200
A
B
-225
B
-270
B
-295
A
-340
A
-390
4 mm
(mV)
APPLIED
POTENTIAL

FIG. 15

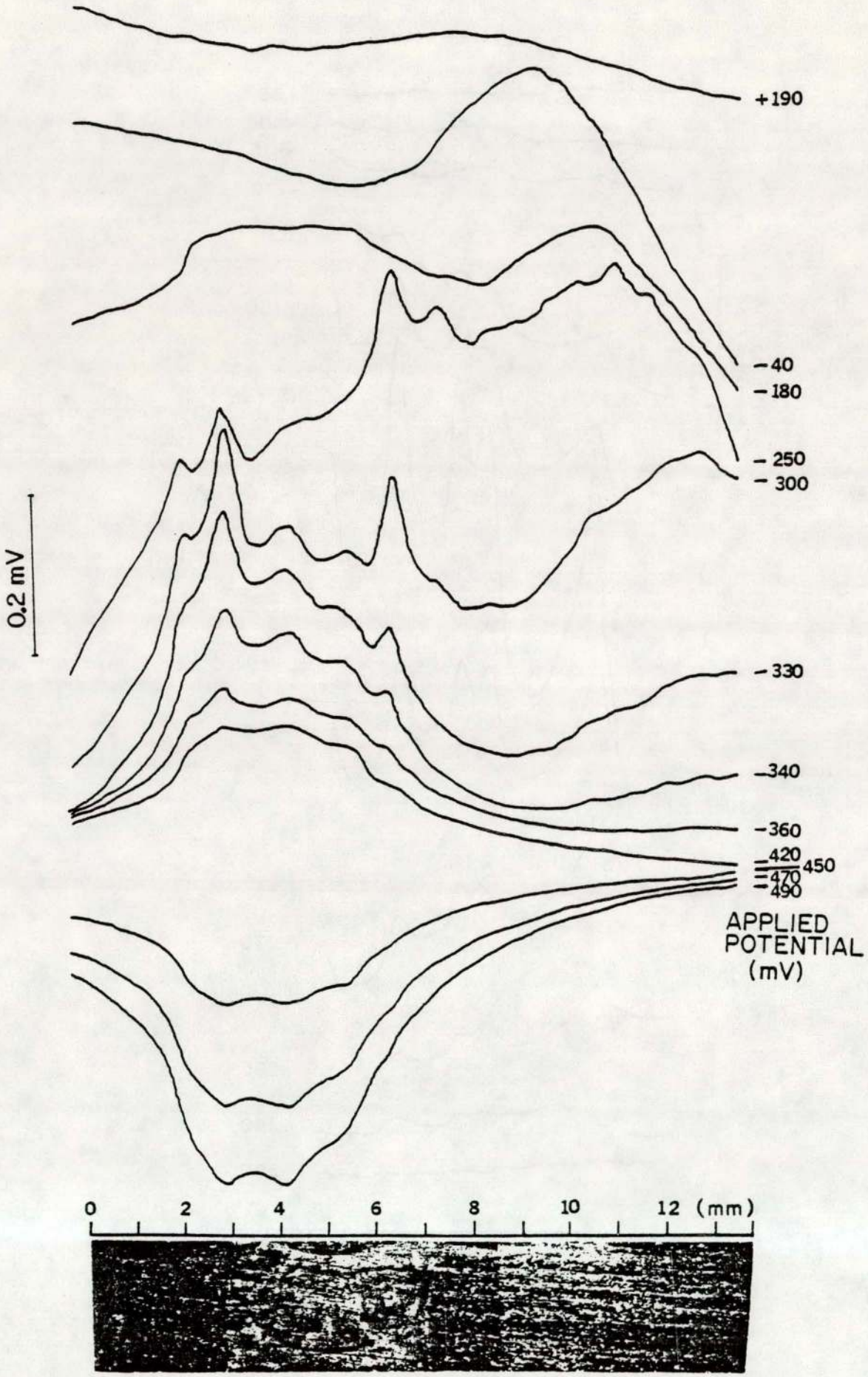
+190
-40
-180
-250
-300
-330
-340
-360
420
450
470
490
APPLIED POTENTIAL (mV)
0.2 mV
0
2
4
6
8
10
12 (mm)

FIG. 16

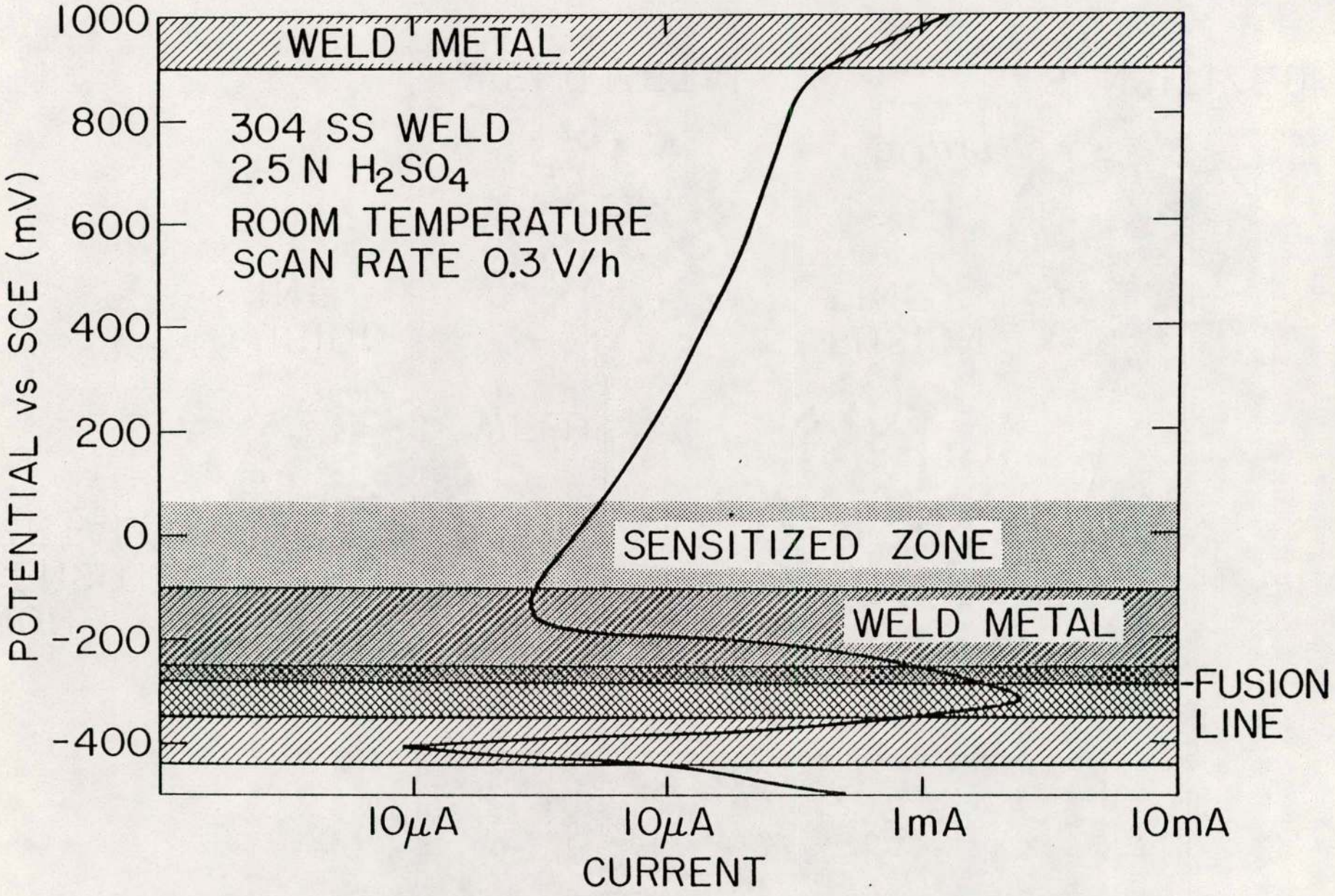
1000
800
600
400
200
0
-200
-400
POTENTIAL vs SCE (mV)
WELD METAL
304 SS WELD
2.5 N H_2SO_4
ROOM TEMPERATURE
SCAN RATE 0.3 V/h
SENSITIZED ZONE
WELD METAL
FUSION LINE
10μA
10μA
1mA
10mA
CURRENT

FIG. 17

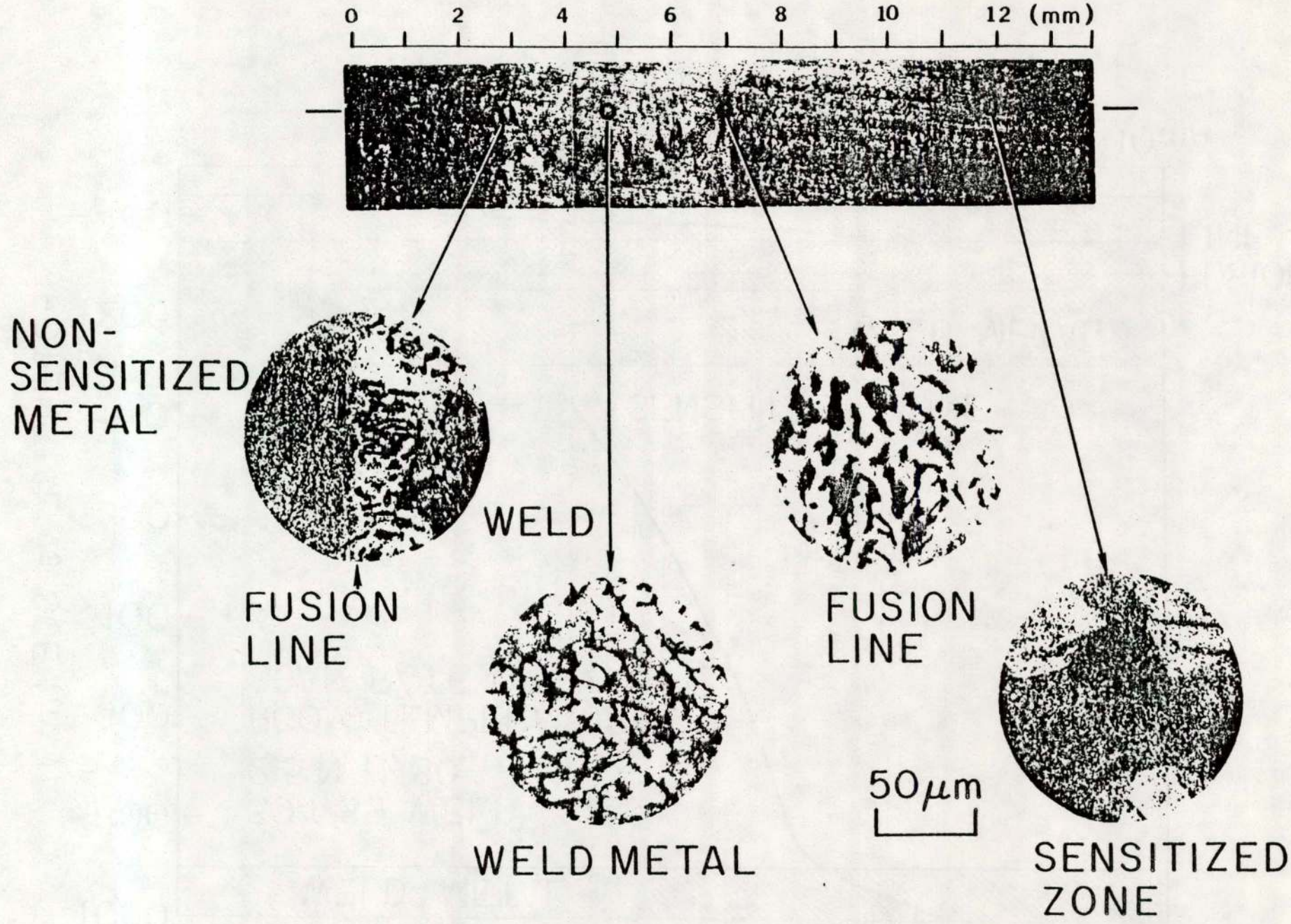
0
2
4
6
8
10
12 (mm)
NON-
SENSITIZED
METAL
FUSION
LINE
WELD
WELD METAL
FUSION
LINE
50μm
SENSITIZED
ZONE

FIG. 18

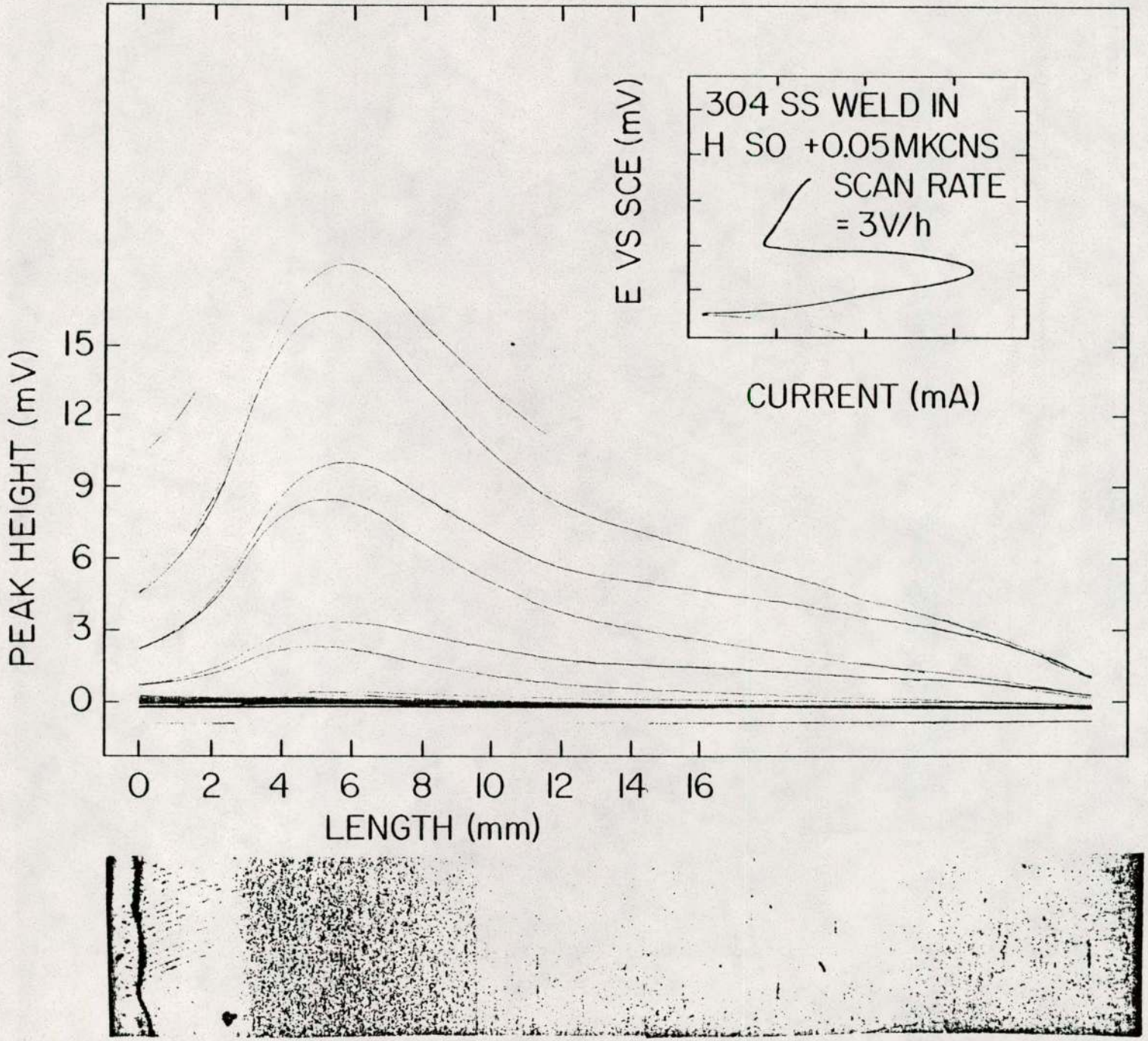

REFERENCE ELECTRODE SCAN OF 304 SS WELD SENSITIZED ZONE

FIG. 19

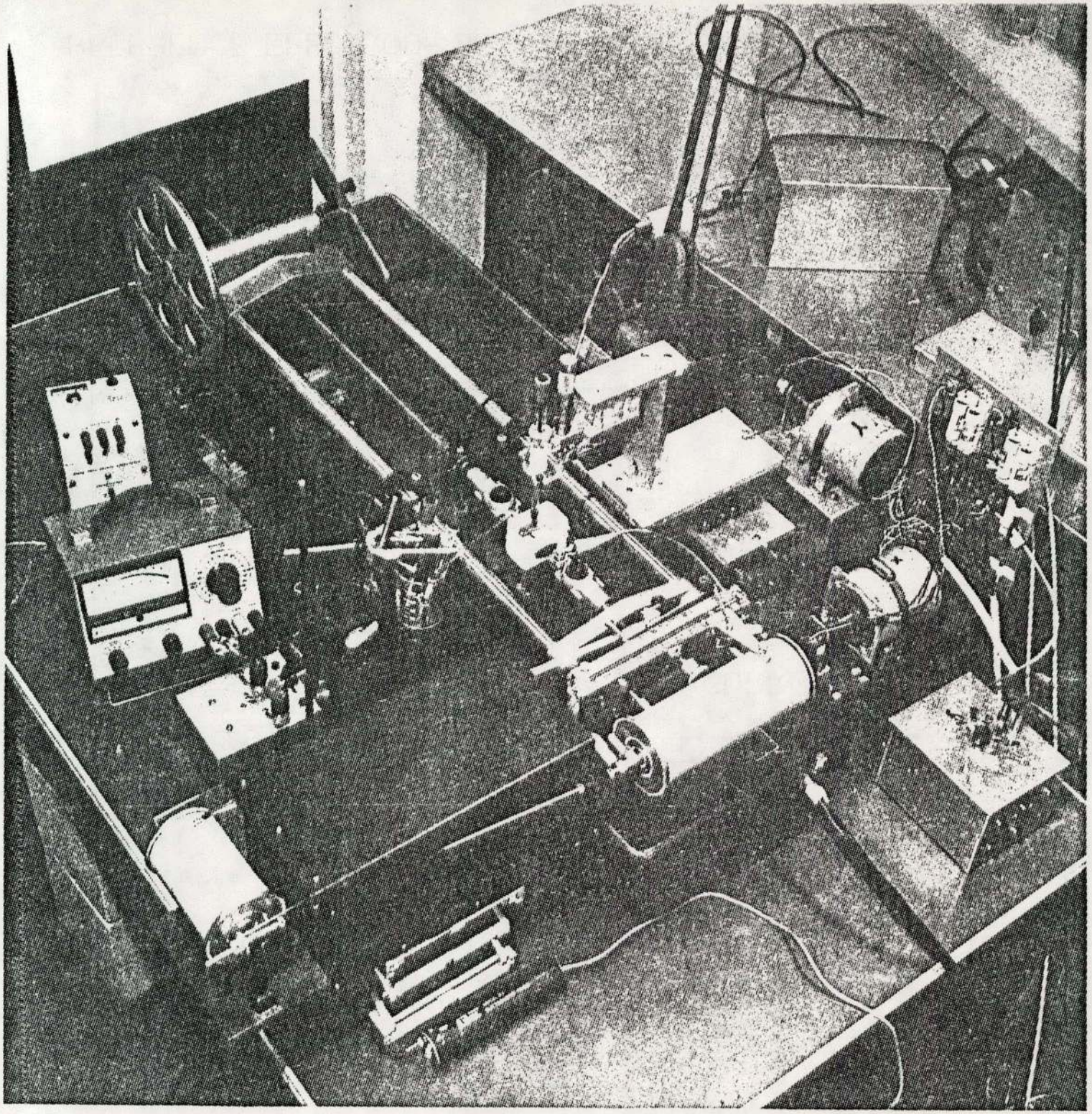

FIG. 20

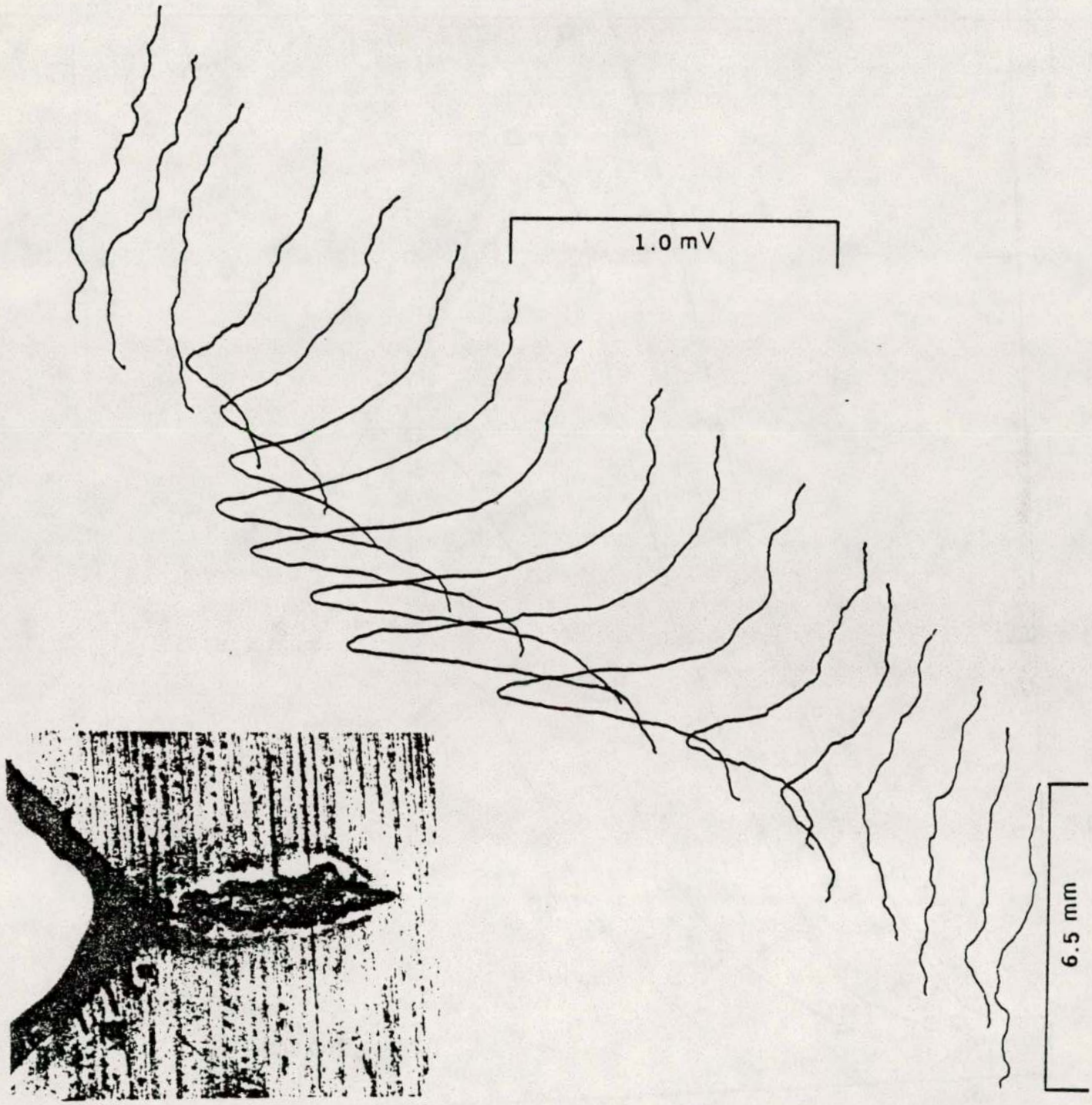

FIG. 21

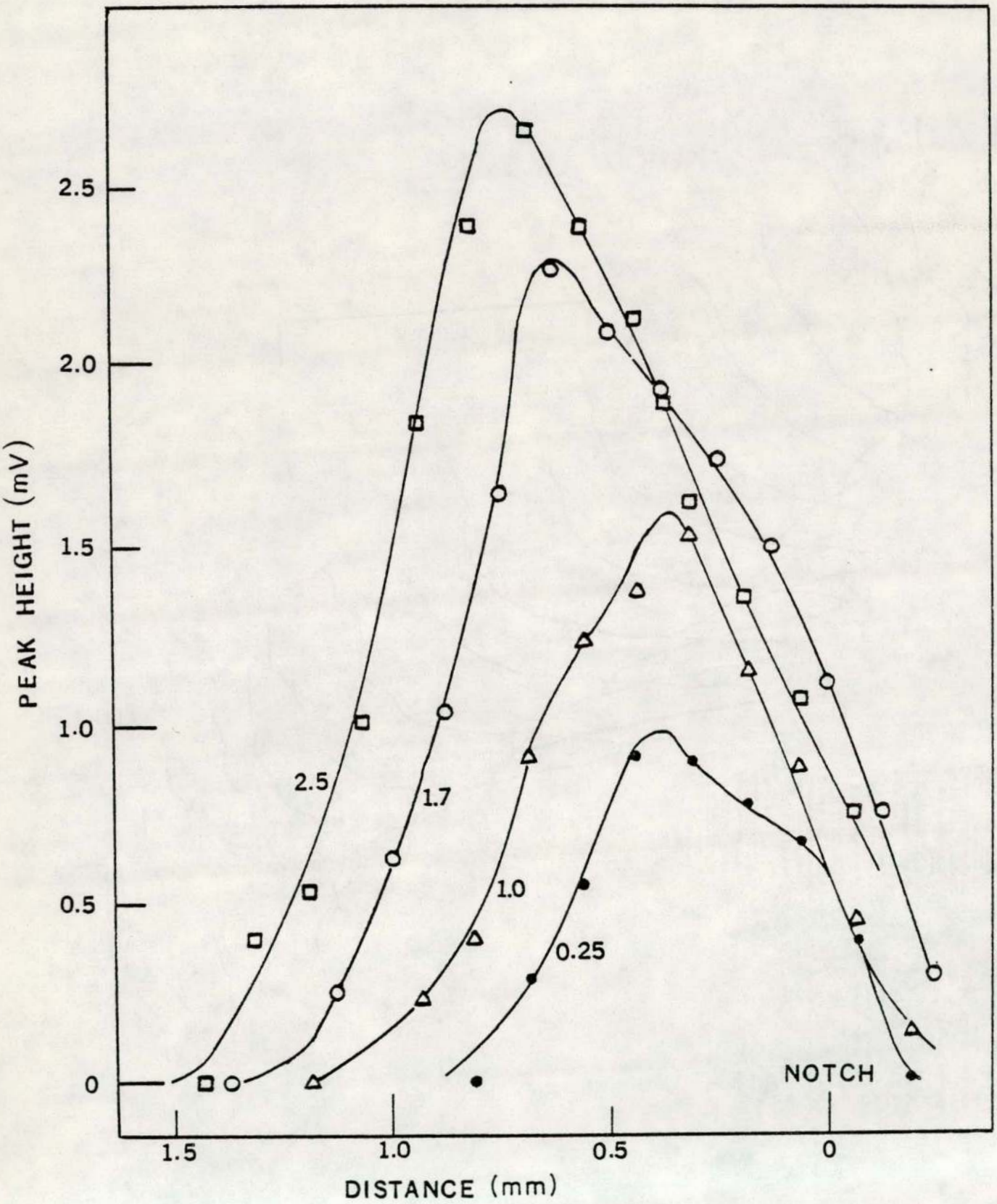
PEAK HEIGHT (mV)
2.5
2.0
1.5
1.0
0.5
0
2.5
1.7
1.0
0.25
NOTCH
1.5
1.0
0.5
0
DISTANCE (mm)

FIG. 22